# Adaptive Robust Tracking Control for Hybrid Models of 3-D Bipedal Robotic Walking under Uncertainties

#### Yan Gu \*

Assistant Professor
Department of Mechanical Engineering
University of Massachusetts Lowell
Lowell, Massachusetts 01854
Email: yan\_gu@uml.edu

# Chengzhi Yuan

Assistant Professor

Department of Mechanical, Industrial and Systems Engineering
University of Rhode Island
Kingston, Rhode Island 02881
Email: cyuan@uri.edu

This paper introduces an adaptive robust trajectory tracking controller design to provably realize stable bipedal robotic walking under parametric and unmodeled uncertainties. Deriving such a controller is challenging mainly because of the highly complex bipedal walking dynamics that are hybrid and involve nonlinear, uncontrolled statetriggered jumps. The main contribution of the study is the synthesis of a continuous-phase adaptive robust tracking control law for hybrid models of bipedal robotic walking by incorporating the construction of multiple Lyapunov functions into the control Lyapunov function. The evolution of Lyapunov function across the state-triggered jumps is explicitly analyzed to construct sufficient conditions that guide the proposed control design for provably guaranteeing the stability and tracking performance of the hybrid system in the presence of uncertainties. Simulation results on fully actuated bipedal robotic walking validate the effectiveness of the proposed approach in walking stabilization under uncertainties.

#### 1 Introduction

Bipedal robots can potentially be used to perform locomotion tasks for a wide range of real-world operations such as home assistance, emergency response, and search and res-

\*Corresponding Author. This material is based upon work supported by the National Science Foundation under Grant No. CMMI-1934280. Any opinions, findings, and conclusions or recommendations expressed in this material are those of the author(s) and do not necessarily reflect the views of the National Science Foundation.

cue. One common control approach towards accomplishing these locomotion tasks is trajectory tracking control. However, a robot's trajectory tracking performance is typically affected by uncertainties such as parametric uncertainties and unmodeled uncertainties [1–3]. Parametric uncertainties exist when the estimated values of the system's model parameters such as a robot's link masses do not match their true values, whereas unmodeled uncertainties include nonlinear functions such as joint frictions. Without proper treatment, these uncertainties can deteriorate tracking performance and even cause instability of bipedal robots, which makes it necessary to design locomotion controllers to mitigate the negative effects of uncertainties.

# 1.1 Related Work on Control Design for Continuous Systems under Uncertainties

To mitigate uncertainties for ensuring the stability and tracking performance of continuous systems, adaptive and robust control has been extensively studied. Adaptive control [4–6] could achieve accurate steady-state tracking under parametric uncertainties by exploiting online adaptation laws to update the estimation of model parameters, but it may not be effective under unmodeled uncertainties such as disturbances [7]. On the contrary, robust control [8, 9] could guarantee satisfactory transient tracking performance under unmodeled uncertainties but cannot guarantee accurate final tracking under parametric uncertainties without relying on high-gain feedback or discontinuous control action.

To combine the complementary advantages of adaptive control and robust control, the inherent conflict of adaptive and robust control design methodologies needs to be resolved. The conflict is that, the estimated model parameters provided by the adaptive control may grow unbounded under unmodeled uncertainties, which will then induce aggressive robust control action for estimation error mitigation. To resolve the conflict, an adaptive robust control approach [10, 11] adds a known bound to the parameter estimation to avoid unbounded parameter drifting. The approach has been used to significantly improve the transient and steady-state trajectory tracking performance for various continuous systems [12–16] in the presence of parametric and unmodeled uncertainties.

# 1.2 Related Work on Control Design for Walking Robots under Uncertainties

By modeling a walking robot as a continuous system, the previously reviewed adaptive control and robust control strategies have been exploited to stabilize and improve the trajectory tracking performance for walking robots [17–22].

However, treating a walking robot as a continuous system in controller design may not be appropriate because bipedal walking robots are inherently hybrid dynamical systems, involving both continuous motions (e.g., foot swinging motions) and state-triggered jumps (e.g., sudden jumps in a robot's joint velocities upon a foot-landing impact) [3, 23–27]. These jumps are particularly difficult to handle in controller design because they are nonlinear and triggered when the system's state satisfies certain conditions (e.g., the swing foot striking the walking surface). Furthermore, they cannot be directly controlled due to their infinitesimal periods of duration [28].

To provably stabilize bipedal walking robots by explicitly addressing their hybrid dynamical behaviors, the Hybrid Zero Dynamics (HZD) framework has been proposed based on orbital stabilization [29] and recently extended to mitigate uncertainties that are prevalent in practical applications [1,2]. Yet, as orbitally stabilizing controllers is not suitable for accurate trajectory tracking [30], these approaches and the underlying stability analysis methods cannot be used to solve the problem of trajectory tracking control.

Beyond the scope of walking controller design, robust trajectory tracking control for general hybrid systems with state-triggered jumps has been investigated based on Lyapunov stability analysis [31]. Still, the previous work does not explicitly analyze the evolution of Lyapunov function across the uncontrolled state-triggered jumps and thus may not be used to directly inform controller design.

To realize reliable trajectory tracking for hybrid systems with state-triggered jumps (including the fully actuated walking robots), we have introduced a Lyapunov-based trajectory tracking controller design based on an explicit analysis of the evolution of the Lyapunov function across state-triggered jumps [32–35]. This controller design has recently been extended and experimentally implemented to achieve provably stable quadrupedal robotic walking on a dynamic rigid surface that rotates in the inertial frame [36]. However, these previous control approaches utilize input-output

linearization and thus may not be effective in guaranteeing a good tracking performance under modeling errors or disturbances. To this end, this study extends our previous control approach to address parametric and unmodeled uncertainties for a class of hybrid systems that include fully actuated bipedal walking robots.

#### 1.3 Contributions

This study addresses the expansion of the adaptive robust controller design methodology from continuous systems to fully actuated hybrid systems with state-triggered jumps for provably guaranteeing the system stability and tracking performance under parametric and unmodeled uncertainties. The specific contributions of this study are:

- (a) To synthesize adaptive robust control laws for fully actuated hybrid systems with state-triggered jumps by incorporating the construction of multiple Lyapunov functions into control Lyapunov function.
- (b) To analyze the stability, tracking performance, and parameter estimation convergence of the closed-loop system by explicitly examining the effects of state-triggered jumps on the evolution of Lyapunov function under uncertainties.
- (c) To provide sufficient conditions based on these analyses under which the proposed control law guarantees the trajectory tracking performance in the presence of parametric and unmodeled uncertainties.
- (d) To demonstrate the validity of the theoretical results through simulations of a fully actuated three-dimensional (3-D) bipedal robot.

Some of the results from this manuscript have been reported in [37]. The new, substantial contributions of this paper include: a) important details and discussions of the proposed controller design and stability analysis are added, including the full proof of Theorem 1 along with all the remarks in Sections 3 and 4; b) the convergence analysis of parameter estimation under no unmodeled uncertainties is added as a new section (Section 5), including Theorem 2 and its proof, which was missing in [37]; c) comparative simulation results between four controllers are presented in Section 6 to illustrate the advantages of the proposed controller, whereas only the simulation results of the proposed controller were presented in [37]; and d) simulation results of the proposed controller under parametric uncertainties are also added in Section 6, which were missing in [37].

The paper is structured as follows. Section 2 presents the full-order hybrid dynamic model of fully actuated bipedal walking robots. Section 3 introduces the continuous-phase adaptive robust control law. Section 4 derives the proposed sufficient closed-loop stability conditions, which can be used to guide the design of adaptive robust controllers for fully actuated hybrid systems. Section 5 explains the analysis of parameter estimation convergence in the absence of uncertain nonlinearities. Section 6 reports the simulation results on 3-D bipedal robotic walking.

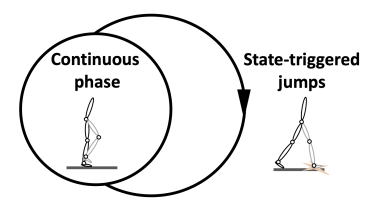


Fig. 1. A directed graph of a complete fully actuated bipedal walking step

## 2 Model

This section presents the hybrid model of bipedal walking dynamics, which serves as a basis for controller derivation.

# 2.1 Hybrid Walking Dynamics

Bipedal walking dynamics are inherently hybrid, involving continuous motion (e.g., foot swinging) as well as state-triggered jumps (e.g., sudden jumps in joint velocities when the swing foot strikes the walking surface), as illustrated in Fig. 1.

The robot is fully actuated when its number of degrees of freedom (DOFs), denoted as n, matches the number of independent actuators, denoted as m. As this study addresses the controller design for fully-actuated walking, the equality m = n holds in the remaining derivation and analysis of the paper.

**Continuous-phase dynamics.** During continuous phases, the robot's dynamic model can be expressed as:

$$\mathbf{M}(\mathbf{q}, \boldsymbol{\beta})\ddot{\mathbf{q}} + \mathbf{C}(\mathbf{q}, \dot{\mathbf{q}}, \boldsymbol{\beta})\dot{\mathbf{q}} + \mathbf{G}(\mathbf{q}, \boldsymbol{\beta}) + \tilde{\mathbf{f}}(t, \mathbf{q}, \dot{\mathbf{q}}) = \mathbf{B}_{tt}\mathbf{u}, \quad (1)$$

where  $\mathbf{q} \in Q$  and  $\mathbf{u} \in U$  are the vectors of joint positions and torques, respectively,  $\boldsymbol{\beta} \in \Omega_{\beta}$  is the vector of model parameters with uncertain values,  $\mathbf{M}: Q \times \Omega_{\beta} \to \mathbb{R}^{n \times n}$  is the inertia matrix,  $\mathbf{C}: TQ \times \Omega_{\beta} \to \mathbb{R}^{n \times n}$  is the Coriolis matrix,  $\mathbf{G}: Q \times \Omega_{\beta} \to \mathbb{R}^n$  is the gravitational term,  $\tilde{\mathbf{f}}: \mathbb{R}^+ \times TQ \to \Omega_{\tilde{f}}$  is the vector of unmodeled uncertainties (e.g., disturbances and joint friction), and  $\mathbf{B}_u \in \mathbb{R}^{n \times n}$  is an input matrix.  $Q \subset \mathbb{R}^n$  is the robot's configuration space when the support foot remains in a full, static contact with the ground and the joint position limits are met. TQ is the tangent space of Q.  $U \subset \mathbb{R}^m$  is the set of the robot's admissible joint torques.  $\Omega_{\beta} \subset \mathbb{R}^{n_p}$  and  $\Omega_{\tilde{f}} \subset \mathbb{R}^n$  are known bounded sets.

The continuous-phase dynamics in Eq. (1) has the following properties [38, 39]:

**Property 1.** The inertia matrix M is symmetric positive definite, and there exist positive numbers  $k_m$  and  $k_M$  such that

$$k_m \mathbf{I}_{n \times n} \le \mathbf{M} \le k_M \mathbf{I}_{n \times n}$$
 (2)

for any  $\mathbf{q} \in Q$  and  $\boldsymbol{\beta} \in \Omega_{\beta}$ , where  $\mathbf{I}_{n \times n} \in \mathbb{R}^{n \times n}$  is an identity matrix.

**Property 2.** The Coriolis matrix  $\mathbf{C}$  can be selected such that the matrix  $\dot{\mathbf{M}} - 2\mathbf{C}$  is skew-symmetric.

**Assumption 1** (Linear Parameterization of Continuous-Phase Dynamics). The model parameters  $\boldsymbol{\beta}$  (e.g., a robot's link masses) linearly parameterize  $\mathbf{M}$ ,  $\mathbf{C}$ , and  $\mathbf{G}$  as:

$$\mathbf{Y}(\mathbf{q},\dot{\mathbf{q}},\dot{\mathbf{q}}_r,\ddot{\mathbf{q}}_r)\boldsymbol{\beta} := \mathbf{M}(\mathbf{q},\boldsymbol{\beta})\ddot{\mathbf{q}}_r + \mathbf{C}(\mathbf{q},\dot{\mathbf{q}},\boldsymbol{\beta})\dot{\mathbf{q}}_r + \mathbf{G}(\mathbf{q},\boldsymbol{\beta})$$
(3)

where  $\mathbf{q}_r \in \mathbb{R}^n$  is any reference vector.

**State-triggered jumps.** When a continuous phase ends, the robot's swing leg strikes the ground causing a discontinuity in the joint positions and velocities. The joint positions of the two legs experience a sudden jump because the swing and the support legs switch roles. The joint velocities may also experience a sudden jump due to the coordinate swap and the rigid-body impact associated with a swing-foot landing. These jumps cannot be directly controlled due to their infinitesimal duration.

The jumps in  $\mathbf{q}$  and  $\dot{\mathbf{q}}$  upon a foot-landing event can be expressed as:

$$\begin{bmatrix} \mathbf{q}^+ \\ \dot{\mathbf{q}}^+ \end{bmatrix} = \mathbf{\Delta}(\mathbf{q}^-, \dot{\mathbf{q}}^-, \boldsymbol{\beta}) \tag{4}$$

where  $\star^+$  and  $\star^-$  represent the values of  $\star$  right before or after an impact, respectively. The derivation of  $\Delta$  is given in [40].

**Switching surface.** A switching surface  $S_q$  describes the occurrence of a swing-foot landing as:

$$S_q := \{ (\mathbf{q}, \dot{\mathbf{q}}, \boldsymbol{\beta}) \in TQ : z_{sw}(\mathbf{q}, \boldsymbol{\beta}) = 0, \\ \dot{z}_{sw}(\mathbf{q}, \dot{\mathbf{q}}, \boldsymbol{\beta}) < 0 \},$$
 (5)

where  $z_{sw}$  is the height of the swing foot above the ground. Note that the switching surface  $S_q$  is not a function of the unknown parameters  $\beta$  if  $\beta$  are link masses.

The overall hybrid system dynamics of a walking robot can be expressed as:

$$\begin{cases} \mathbf{M}\ddot{\mathbf{q}} + \mathbf{C}\dot{\mathbf{q}} + \mathbf{G} + \tilde{\mathbf{f}} = \mathbf{B}_{u}\mathbf{u}, & \text{if } (\mathbf{q}^{-}, \dot{\mathbf{q}}^{-}) \notin S_{q}; \\ \begin{bmatrix} \mathbf{q}^{+} \\ \dot{\mathbf{q}}^{+} \end{bmatrix} = \mathbf{\Delta}, & \text{if } (\mathbf{q}^{-}, \dot{\mathbf{q}}^{-}) \in S_{q}. \end{cases}$$
(6)

# 2.2 Boundedness of Model Parameters and Unmodeled Nonlinearities

Given that uncertainties, such as unmodeled joint frictions and unknown link masses, are usually bounded during real-world applications [41], it is assumed in this study that uncertainties are bounded:

**Assumption 2** (Boundedness of Model Parameters). The actual value of the model parameter  $\beta$  is bounded by known vectors  $\beta_{\min}$  and  $\beta_{\max}$ :

$$\boldsymbol{\beta} \in [\boldsymbol{\beta}_{\min}, \boldsymbol{\beta}_{\max}]. \tag{7}$$

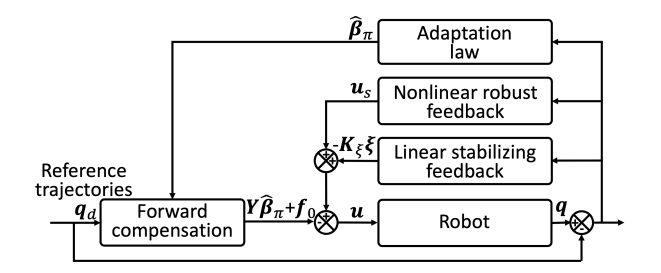


Fig. 2. Block diagram of a continuous adaptive robust control law

**Assumption 3** (Boundedness of Unmodeled Nonlinearities). The unmodeled nonlinearities  $\tilde{\mathbf{f}}$  are bounded by a known function  $h_f(t, \mathbf{q}, \dot{\mathbf{q}})$ :

$$\|\tilde{\mathbf{f}}(t,\mathbf{q},\dot{\mathbf{q}})\| \le h_f(t,\mathbf{q},\dot{\mathbf{q}}).$$
 (8)

# 3 Continuous Adaptive Robust Control

This section presents an adaptive robust control approach that stabilizes the *continuous* phase of the uncertain hybrid system in Eq. (6). To guarantee the stability and tracking performance of the overall *hybrid* system, sufficient conditions are derived in Section 4 for guiding the gain tuning of the control law.

Without loss of generality, we choose the joint positions  $\mathbf{q}$  as the variables to be controlled. Note that a fully actuated system has full control authority over all of its n joint positions and thus can directly command all joints to track n desired trajectories  $\mathbf{q}_d(t)$ . The tracking error is  $\mathbf{e} = \mathbf{q} - \mathbf{q}_d$ .

**Control Objective.** To derive a control law that stabilizes the uncertain hybrid system in Eq. (6) and guarantees a bounded final tracking error for achieving provably stable bipedal robotic walking.

We propose to achieve this control objective by extending the continuous adaptive robust controller (ARC) design methodology [42] from continuous systems to fully actuated hybrid systems with state-triggered jumps, because a) only the continuous phase of the hybrid system in Eq. (6) can be directly driven but not the jumps and b) ARC is effective in addressing uncertainties for continuous systems as reviewed in Section 1.

A continuous ARC consists of a nonlinear robust feedback term, a parameter adaptation law, a feedforward term, and a linear stabilizing feedback term (see Fig. 2). The robust feedback term mitigates the effects of unmodeled nonlinear uncertainties. The parameter adaptation law estimates the actual values of the model parameters. The feedforward term compensates for the nonlinear dynamics using estimated parameter values. The linear stabilizing feedback term stabilizes the continuous-phase system.

# 3.1 Robust Feedback

The robust feedback term of an ARC is crucial to guarantee the stability and transient tracking performance of a continuous system under unmodeled uncertainties. We choose

sliding mode control (SMC) [42] as the robust feedback term because previous work [19] has validated its enhanced performance in rejecting uncertainties for legged locomotion.

An SMC drives a system's state to a hypersurface in the state space (i.e., a sliding mode). To enhance the tracking performance of the continuous-phase system within the sliding mode, we form the SMC using a dynamic compensator [42]:

$$\begin{cases} \dot{\mathbf{x}}_c = \mathbf{A}_c \mathbf{x}_c + \mathbf{B}_c \mathbf{e}; \\ \mathbf{y}_c = \mathbf{C}_c \mathbf{x}_c + \mathbf{D}_c \mathbf{e}, \end{cases}$$
(9)

where  $\mathbf{x}_c$  and  $\mathbf{y}_c$  are the state and the output of the dynamic compensator, respectively.  $\mathbf{A}_c \subset \mathbb{R}^{n_c \times n_c}$ ,  $\mathbf{B}_c \subset \mathbb{R}^{n_c \times n_c}$ ,  $\mathbf{C}_c \subset \mathbb{R}^{n \times n_c}$ , and  $\mathbf{D}_c \subset \mathbb{R}^{n \times n}$  are matrices that define the dynamic compensator  $(n_c = n)$ . These matrices are chosen such that  $(\mathbf{A}_c, \mathbf{B}_c, \mathbf{C}_c, \mathbf{D}_c)$  is observable and controllable.

Introduce a vector  $\boldsymbol{\xi} \in \mathbb{R}^n$  to define the sliding mode as  $\boldsymbol{\xi} = \mathbf{0}$ , and choose  $\boldsymbol{\xi}$  as:

$$\boldsymbol{\xi} = \dot{\mathbf{q}} - \dot{\mathbf{q}}_r,\tag{10}$$

where  $\dot{\mathbf{q}}_r := \dot{\mathbf{q}}_d - \mathbf{y}_c$ . Then, the goal of the SMC is to guarantee that the system state remains within the sliding mode, that is,  $\boldsymbol{\xi}$  remains zero.

Let  $h_s$  be the sum of the bounds of unmodeled uncertainties and parameter estimation error. Then,

$$h_s(t, \mathbf{q}, \dot{\mathbf{q}}, \dot{\mathbf{q}}_r, \ddot{\mathbf{q}}_r) := h_f(t, \mathbf{q}, \dot{\mathbf{q}}) + h_\beta(\mathbf{q}, \dot{\mathbf{q}}, \dot{\mathbf{q}}_r, \ddot{\mathbf{q}}_r), \tag{11}$$

where the definition of  $h_{\beta}$  is given in Section 3.2. The ideal SMC is then  $-h_s \frac{\xi}{\|\xi\|}$ .

To reduce the chattering effect caused by the discontinuity of the ideal SMC, the robust feedback term is designed as:

$$\mathbf{u}_r = \mathbf{h}(-h_s \frac{\boldsymbol{\xi}}{\|\boldsymbol{\xi}\|}),\tag{12}$$

where  $\mathbf{h}(-h_s \frac{\boldsymbol{\xi}}{\|\boldsymbol{\xi}\|})$  is a continuous approximation of the ideal SMC with an approximation error  $\varepsilon(t)$  ( $\varepsilon(t) > 0$  for any t > 0).

A valid choice of the continuous approximation **h** should satisfy the following two conditions [42]:

(C1) 
$$\boldsymbol{\xi}^T \mathbf{h}(-h_s \frac{\boldsymbol{\xi}}{\|\boldsymbol{\xi}\|}) \leq 0.$$
  
(C2)  $h_s \|\boldsymbol{\xi}\| + \boldsymbol{\xi}^T \mathbf{h}(-h_s \frac{\boldsymbol{\xi}}{\|\boldsymbol{\xi}\|}) \leq \varepsilon(t).$ 

Here, we utilize the following definition of **h** among others [4,43] because it is relatively easy to implement thanks

to its simple expression:

$$\mathbf{h}(-h_s \frac{\boldsymbol{\xi}}{\|\boldsymbol{\xi}\|}) := \begin{cases} -\mathbf{K}_s \boldsymbol{\xi} & \text{if } \|\boldsymbol{\xi}\| \leq \phi_h \\ -h_s \frac{\boldsymbol{\xi}}{\|\boldsymbol{\xi}\|} & \text{if } \|\boldsymbol{\xi}\| \geq (1 + \varepsilon_2)\phi_h \\ -(1 - c_1)\mathbf{K}_s \boldsymbol{\xi} - c_1 h_s \frac{\boldsymbol{\xi}}{\|\boldsymbol{\xi}\|} & \text{elsewhere} \end{cases}$$

$$\tag{13}$$

where  $\mathbf{K}_s \in \mathbb{R}^{n \times n}$  is any symmetric positive definite matrix, and  $\varepsilon_1$  and  $\varepsilon_2$  are any positive scalars.  $\phi_h := \frac{\phi}{h_s(t,\mathbf{q},\dot{\mathbf{q}},\dot{\mathbf{q}}_r,\dot{\mathbf{q}}_r)+\varepsilon_1}$ , where  $\phi(t)$  is any positive scalar function on t>0.  $c_1=\frac{\|\boldsymbol{\xi}\|-\phi_h}{\varepsilon_2\phi_h}$ . Then, the approximation error  $\varepsilon$  is  $\varepsilon(t)=(1+\varepsilon_2)\phi_h(t)$ .

**Remark 1** (Reset of  $\boldsymbol{\xi}$  at  $T_k^+$ ). The state variable  $\mathbf{x}_c$  of the dynamic compensator can be arbitrarily designed at the initial moment of any continuous phase. Let  $T_k$  be the initial timing of the  $k^{th}$  walking step  $(k \in \{1,2,...\})$ . Selecting  $\mathbf{C}_c$  as a nonsinguar matrix, we can reset the value of  $\mathbf{x}_c$  as

$$\mathbf{x}_{c}(T_{k}^{+}) = -\mathbf{C}_{c}^{-1}(\dot{\mathbf{e}}(T_{k}^{+}) + \mathbf{D}_{c}\mathbf{e}(T_{k}^{+})). \tag{14}$$

Accordingly,  $\xi$  is reset to zero whenever a new walking step begins, that is,

$$\boldsymbol{\xi}(T_k^+) = \dot{\mathbf{e}}(T_k^+) + \mathbf{y}_c(T_k^+) = \mathbf{0},$$
 (15)

which helps reduce the unpleasant transient response of  $\xi$ .

**Remark 2** (Response within Sliding Mode). The transfer function matrix from  $\boldsymbol{\xi}$  to  $\mathbf{e}$  is  $(s\mathbf{I}_{n\times n}+\mathbf{G}_c(s))^{-1}$ , where  $\mathbf{G}_c(s):=\mathbf{C}_c(s\mathbf{I}_{n_c\times n_c}-\mathbf{A}_c)^{-1}\mathbf{B}_c+\mathbf{D}_c$ . By carefully assigning the poles of the matrix, the desired response within the sliding mode can be achieved.

# 3.2 Parameter Adaptation

The parameter adaption law estimates the actual values of the uncertain model parameters  $\beta$ . By reducing the modeling error, it enhances the final tracking accuracy without replying on high-gain feedback control. With the estimated parameters, a feedforward term can be formed to compensate for the nonlinear continuous-phase dynamics, as shown in Fig. 2.

Let  $\hat{\boldsymbol{\beta}} \in \Omega_{\beta}$  be the estimate of  $\boldsymbol{\beta}$ . Let  $\tilde{\boldsymbol{\beta}} := \hat{\boldsymbol{\beta}} - \boldsymbol{\beta}$  be the parameter estimation error. The parameter adaptation law is expressed as:

$$\dot{\hat{\boldsymbol{\beta}}} = -\Gamma \boldsymbol{\tau}.\tag{16}$$

The adaptation function  $\tau$  is defined as:

$$\boldsymbol{\tau} = \mathbf{Y}^T(\mathbf{q}, \dot{\mathbf{q}}, \dot{\mathbf{q}}_r, \ddot{\mathbf{q}}_r)\boldsymbol{\xi}. \tag{17}$$

This parameter estimation law can cause an unbounded estimation error under unmodeled uncertainty  $\tilde{\mathbf{f}}$ . However,

the robust feedback term given in Section 3.1 demands the knowledge of the estimation error bound. The key to resolve this conflict is to impose a bound on the parameter estimation  $\hat{\beta}$ . To this end, different modifications of  $\hat{\beta}$  have been proposed [42]. We choose to utilize a smooth modification so as to allow explicit analysis of the convergence of  $\hat{\beta}$  based on Lyapunov theory in Section 5.

Let  $\pi(\hat{\beta})$  be a smooth projection of  $\hat{\beta}$  with sufficiently smooth, bounded derivatives and satisfying the conditions below:

(C3) 
$$\pi(\hat{\boldsymbol{\beta}}) = \hat{\boldsymbol{\beta}} \text{ if } \hat{\boldsymbol{\beta}} \in \Omega_{\boldsymbol{\beta}}.$$

(C4)  $\boldsymbol{\pi}(\hat{\boldsymbol{\beta}}) \in \Omega_{\hat{\boldsymbol{\beta}}} := [\boldsymbol{\beta}_{\min} - \boldsymbol{\varepsilon}_{\boldsymbol{\beta}} \quad \boldsymbol{\beta}_{\max} + \boldsymbol{\varepsilon}_{\boldsymbol{\beta}}] \text{ if } \hat{\boldsymbol{\beta}} \in \mathbb{R}^{n_p},$  where  $\boldsymbol{\varepsilon}_{\boldsymbol{\beta}} \in \mathbb{R}^{n_p}$  is a known vector of small positive numbers.

An example of the smooth projection mapping  $\pi(\hat{\beta})$  [11] is:

$$\pi_{i}(\hat{\beta}_{i}) = \begin{cases} \beta_{imin} + \varepsilon_{i\beta} (1 - e^{-\frac{\hat{\beta}_{i} - \beta_{imin}}{\varepsilon_{i\beta}}}) & \text{if } \hat{\beta}_{i} < \beta_{imin} \\ \beta_{imax} + \varepsilon_{i\beta} (1 - e^{-\frac{\hat{\beta}_{i} - \beta_{imax}}{\varepsilon_{i\beta}}}) & \text{if } \hat{\beta}_{i} > \beta_{imax} \\ \hat{\beta}_{i} & \text{elsewhere} \end{cases},$$

where the scalars  $\pi_i$ ,  $\hat{\beta}_i$ ,  $\beta_{imin}$ ,  $\beta_{imax}$ , and  $\varepsilon_{i\beta}$  are the  $i^{th}$  elements of the vectors  $\pi$ ,  $\hat{\beta}$ ,  $\beta_{min}$ ,  $\beta_{max}$ , and  $\varepsilon_{\beta}$ , respectively.

To simplify notations, define  $\hat{\boldsymbol{\beta}}_{\pi} := \boldsymbol{\pi}(\hat{\boldsymbol{\beta}})$  and  $\tilde{\boldsymbol{\beta}}_{\pi} := \hat{\boldsymbol{\beta}}_{\pi} - \boldsymbol{\beta}$ . From Assumption 2 and the conditions (C3) and (C4), we have:

$$\|\mathbf{Y}(\mathbf{q},\dot{\mathbf{q}},\dot{\mathbf{q}}_r,\ddot{\mathbf{q}}_r)\tilde{\boldsymbol{\beta}}_{\pi}\| \le h_{\beta}(\mathbf{q},\dot{\mathbf{q}},\dot{\mathbf{q}}_r,\ddot{\mathbf{q}}_r). \tag{18}$$

An example of the bound  $h_{\beta}$  is:

$$h_{\beta} := \|\mathbf{Y}(\mathbf{q}, \dot{\mathbf{q}}, \dot{\mathbf{q}}_r, \ddot{\mathbf{q}}_r)\|\beta_{M} := \|\mathbf{Y}(\mathbf{q}, \dot{\mathbf{q}}, \dot{\mathbf{q}}_r, \ddot{\mathbf{q}}_r)\|\|\boldsymbol{\beta}_{\max} - \boldsymbol{\beta}_{\min} + \boldsymbol{\varepsilon}_{\beta}\|.$$
(19)

**Remark 3** (Boundedness of  $\|\mathbf{Y}\|$ ). For a general legged robot with all joints revolute, the boundedness of  $\|\mathbf{Y}\|$  can be guaranteed as follows. The norms  $\|\mathbf{M}(\mathbf{q}, \boldsymbol{\beta})\|$ ,  $\|\mathbf{C}(\mathbf{q}, \dot{\mathbf{q}}, \boldsymbol{\beta})\|$ , and  $\|\mathbf{G}(\mathbf{q}, \boldsymbol{\beta})\|$  are all bounded within the robot's joint limit (i.e.,  $(\mathbf{q}, \dot{\mathbf{q}}) \in TQ$ ) [39]. Suppose the reference trajectory  $\mathbf{q}_d$  is planned as physically feasible (i.e.,  $\mathbf{q}_d$ ,  $\dot{\mathbf{q}}_d$ , and  $\ddot{\mathbf{q}}_d$  are all bounded). Then, the trajectory  $\mathbf{q}_r$ ,  $\dot{\mathbf{q}}_r$ , and  $\ddot{\mathbf{q}}_r$  are also bounded within the robot's joint and actuation limits. Thus,  $\|\mathbf{Y}(\mathbf{q}, \dot{\mathbf{q}}_r, \ddot{\mathbf{q}}_r)\|$  is bounded.

# 3.3 Overall Control Law

In summary, the expression of a continuous ARC is:

$$\mathbf{u} = \mathbf{B}_{u}^{-1} (\mathbf{u}_{r} + \mathbf{Y}(\mathbf{q}, \dot{\mathbf{q}}, \dot{\mathbf{q}}_{r}, \ddot{\mathbf{q}}_{r}) \hat{\boldsymbol{\beta}}_{\pi} - \mathbf{K}_{\xi} \boldsymbol{\xi}), \tag{20}$$

where  $\mathbf{K}_{\xi} \in \mathbb{R}^{n \times n}$  is any symmetric positive definite matrix. The robust feedback term  $\mathbf{u}_r$  and the adaptation law for  $\hat{\boldsymbol{\beta}}$  are

given in Eqs. (12) and (16), respectively.

With properly selected control gains of the ARC, the stability and tracking performance of the continuous phases of the uncertain hybrid systems in Eq. (6) can be ensured. Yet, the state-triggered jumps remain uncontrolled, and thus the ARC may not be effective in stabilizing the overall hybrid system. Therefore, in Section IV, we derive sufficient conditions under which the continuous ARC provably guarantees the stability and tracking performance for the overall hybrid system under uncertainties.

# 4 Closed-loop Stability Analysis

This section analyzes the stability of the uncertain hybrid systems with state-triggered jumps in Eq. (6) under the proposed continuous ARC. The outcome of the analysis is a set of sufficient conditions that can be used to guide the selection and tuning of control gains for guaranteeing the stability and tracking performance of the closed-loop hybrid system.

The key of the proposed stability analysis is to explicitly analyze the effects of state-triggered jumps on the system stability and tracking performance. Such an explicit analysis is necessary as the jumps are uncontrolled because of their infinitesimal duration. However, the analysis is complex mainly because the occurrence timing of these jumps is an implicit function of state.

Define 
$$\mathbf{z} := \begin{bmatrix} \mathbf{x}_c \\ \mathbf{e} \end{bmatrix}$$
. Then,

$$\begin{cases} \dot{\mathbf{z}} = \mathbf{A}_z \mathbf{z} + \mathbf{B}_z \boldsymbol{\xi}; \\ \mathbf{y}_z = \mathbf{C}_z \mathbf{z}, \end{cases}$$
 (21)

where 
$$\mathbf{A}_z := \begin{bmatrix} \mathbf{A}_c & \mathbf{B}_c \\ -\mathbf{C}_c & -\mathbf{D}_c \end{bmatrix}$$
,  $\mathbf{B}_z := \begin{bmatrix} \mathbf{0} \\ \mathbf{I}_{n \times n} \end{bmatrix}$ , and  $\mathbf{C}_z := \begin{bmatrix} \mathbf{0} & \mathbf{I}_{n \times n} \end{bmatrix}$ . Let the system state be

$$\mathbf{x} := \begin{bmatrix} \mathbf{z} \\ \mathbf{\xi} \end{bmatrix}$$

with  $\|\mathbf{x}\| := \sqrt{\|\mathbf{z}\|^2 + \|\mathbf{\xi}\|^2}$ .

The closed-loop hybrid system under the continuous ARC can be expressed as:

$$\begin{cases}
\mathbf{M}\dot{\boldsymbol{\xi}} + (\mathbf{C} + \mathbf{K}_{\boldsymbol{\xi}})\boldsymbol{\xi} = \mathbf{h}(-h_{s}\frac{\boldsymbol{\xi}}{\|\boldsymbol{\xi}\|}) + \mathbf{Y}\tilde{\boldsymbol{\beta}}_{\pi} - \tilde{\mathbf{f}} \\
\dot{\mathbf{z}} = \mathbf{A}_{z}\mathbf{z} + \mathbf{B}_{z}\boldsymbol{\xi} \\
\begin{bmatrix} \boldsymbol{\xi}^{+} \\ \mathbf{z}^{+} \end{bmatrix} = \begin{bmatrix} \mathbf{0} \\ \mathbf{\Delta}_{z} \end{bmatrix} & \text{if } (t, \mathbf{x}^{-}, \boldsymbol{\beta}) \notin S_{x}.
\end{cases}$$
(22)

The expression of  $\Delta_z(t, \mathbf{x}^-, \boldsymbol{\beta})$  can be obtained from Eqs. (4), (9) and (14). The expression of  $S_x$  can be obtained from Eqs. (5) and (10). Note that  $\Delta_z$  is explicitly time-dependent because the reference trajectory  $\mathbf{q}_d$  is explicitly time-dependent.

**Theorem 1.** The continuous-phase tracking control law in Eq. (20) stabilizes the hybrid system in Eq. (22) locally if its

control gains are selected such that:

- (C5) The matrix  $A_z$  in Eq. (22) is Hurwitz.
- (C6) The state **x** converges sufficiently fast during continuous phases.

**Proof:** Let  $V_{\xi}(\boldsymbol{\xi})$  and  $V_{z}(\mathbf{z})$  be the Lyapunov function candidates for  $\boldsymbol{\xi}$  and  $\mathbf{z}$ , respectively:

$$V_{\xi} = \frac{1}{2} \boldsymbol{\xi}^T \mathbf{M} \boldsymbol{\xi} \text{ and } V_z = \mathbf{z}^T \mathbf{P}_z \mathbf{z}.$$
 (23)

Because the matrix  $\mathbf{A}_z$  is Hurwitz by the condition (C5), the matrix  $\mathbf{P}_z \in \mathbb{R}^{n_c \times n_c}$  can be obtained by solving the following Lyapunov equation [30]:

$$\mathbf{A}_{z}^{T}\mathbf{P}_{z} + \mathbf{P}_{z}\mathbf{A}_{z} = -\mathbf{Q}_{z}, \tag{24}$$

where  $\mathbf{Q}_z \in \mathbb{R}^{n_c \times n_c}$  is any symmetric positive definite matrix. The total Lyapunov function is defined as:

$$V_t(\mathbf{x}) = V_{\mathcal{E}}(\boldsymbol{\xi}) + V_z(\mathbf{z}). \tag{25}$$

The derivation of the stability conditions is based on the incorporation of the construction of multiple Lyapunov functions into the control Lyapunov functions  $V_t$ . By the stability theory via the construction of multiple Lyapunov functions [44], a hybrid system is stable if two conditions are met: a) the value of the Lyapunov function is decreasing during continuous phases and b) the values of the Lyapunov function just after each jump form a sequence that strictly decreases.

**Evolution of**  $V_t$  **during continuous phases.** Following the above conditions, we first analyze the evolution of the Lyapunov function  $V_t$  during continuous phases. Define

$$k_1 := \lambda_{\min}(\mathbf{P}_z), \ k_2 := \lambda_{\max}(\mathbf{P}_z), \ \text{and} \ k_3 := \frac{\lambda_{\min}(\mathbf{Q}_z)}{k_2}, \ (26)$$

with  $\lambda_{\min}(\star)$  and  $\lambda_{\min}(\star)$  being the largest and the smallest eigenvalues of  $\star$ , respectively. Within the continuous phase of the  $k^{th}$  walking step, i.e.,  $t \in (T_k, T_{k+1}]$  with  $T_k$  ( $k \in \{1, 2, ...\}$ ) the initial timing of the  $k^{th}$  walking step, we know from Eq. 23 that

$$k_1 \|\mathbf{z}\|^2 \le V_z \le k_2 \|\mathbf{z}\|^2 \tag{27}$$

and

$$\dot{V}_{z} \le -k_3 V_{z} \tag{28}$$

for any  $\mathbf{z}(0) \in \mathbb{R}^{n_c+n}$ .

From Eqs. (2) and (23), there exists a positive number  $r_{\xi}$  such that

$$\frac{1}{2}k_m\|\boldsymbol{\xi}\|^2 \le V_{\boldsymbol{\xi}} \le \frac{1}{2}k_M\|\boldsymbol{\xi}\|^2 \tag{29}$$

holds for all  $\xi(0) \in \{\xi : ||\xi|| \le r_{\xi}\}.$ 

From Property 2,  $\dot{\mathbf{M}} - 2\mathbf{C}$  is skew symmetric. Then,

$$\frac{1}{2}\boldsymbol{\xi}^T \dot{\mathbf{M}} \boldsymbol{\xi} = \boldsymbol{\xi}^T \mathbf{C} \boldsymbol{\xi}. \tag{30}$$

From Eqs. (22), (25), and (30),

$$\dot{V}_{\xi} = \boldsymbol{\xi}^{T} \mathbf{M} \dot{\boldsymbol{\xi}} + \frac{1}{2} \boldsymbol{\xi}^{T} \dot{\mathbf{M}} \boldsymbol{\xi} 
= \boldsymbol{\xi}^{T} (\mathbf{M} \dot{\boldsymbol{\xi}} + \mathbf{C} \boldsymbol{\xi}) 
= \boldsymbol{\xi}^{T} (\mathbf{Y} \tilde{\boldsymbol{\beta}}_{\pi} - \tilde{\mathbf{f}} - \mathbf{K}_{\xi} \boldsymbol{\xi} + \mathbf{h} (-h_{s} \frac{\boldsymbol{\xi}}{\|\boldsymbol{\xi}\|})) 
\leq \|\boldsymbol{\xi}\| (\|\mathbf{Y} \tilde{\boldsymbol{\beta}}_{\pi}\| + \|\tilde{\mathbf{f}}\|) - \boldsymbol{\xi}^{T} \mathbf{K}_{\xi} \boldsymbol{\xi} + \boldsymbol{\xi}^{T} \mathbf{h} (-h_{s} \frac{\boldsymbol{\xi}}{\|\boldsymbol{\xi}\|})).$$
(31)

Therefore, from the condition (C2) and Eqs. (8), (11), and (18), we have

$$\dot{V}_{\xi} \le -\boldsymbol{\xi}^T \mathbf{K}_{\xi} \boldsymbol{\xi} + \boldsymbol{\varepsilon}(t) \le -\lambda_{\xi} V_{\xi} + \boldsymbol{\varepsilon}(t), \tag{32}$$

where

$$\lambda_{\xi} := \frac{2\lambda_{\min}(\mathbf{K}_{\xi})}{k_{M}}.$$
 (33)

Hence, for all  $\mathbf{x}(0) \in B_{r_{\xi}}(\mathbf{0}) := \{\mathbf{x} : ||\mathbf{x}|| \le r_{\xi}\}$ , the total control Lyapunov function  $V_t$  satisfies

$$k_{t1} \|\mathbf{x}\|^2 \le V_t(\mathbf{x}) \le k_{t2} \|\mathbf{x}\|^2$$
 (34)

and

$$\dot{V}_t \le -k_{t3}V_t + \varepsilon(t) \tag{35}$$

within the continuous phase of the  $k^{th}$  walking step, where

$$k_{t1} := \min(k_1, \frac{k_m}{2}), \ k_{t2} := \max(k_2, \frac{k_M}{2}),$$
  
and  $k_{t3} := \min(k_3, \lambda_{\xi}).$  (36)

**Evolution of**  $V_t$  **across jumps.** Because  $\xi$  is reset to zero at the initial timing of each walking step,  $V_{\xi}$  is reset to zero. Hence, only the evolution of  $V_z$  across the jump  $\Delta_z$  needs to be analyzed.

To simplify notations,  $\star(T_k^-)$  and  $\star(T_k^+)$  are denoted as  $\star|_k^-$  and  $\star|_k^+$ , respectively, in the following analysis.

The norm of **z** after an impact at  $T_{k+1}^-$  can be estimated as:

$$\|\mathbf{z}|_{k+1}^{+}\| = \|\boldsymbol{\Delta}_{z}(T_{k+1}, \mathbf{x}|_{k+1}^{-}, \boldsymbol{\beta})\|$$

$$\leq \|\boldsymbol{\Delta}_{z}(T_{k+1}, \mathbf{x}|_{k+1}^{-}, \boldsymbol{\beta}) - \boldsymbol{\Delta}_{z}(\tau_{k+1}, \mathbf{x}|_{k+1}^{-}, \boldsymbol{\beta})\|$$

$$+ \|\boldsymbol{\Delta}_{z}(\tau_{k+1}, \mathbf{x}|_{k+1}^{-}, \boldsymbol{\beta}) - \boldsymbol{\Delta}_{z}(\tau_{k+1}, \mathbf{0}, \boldsymbol{\beta})\|$$

$$+ \|\boldsymbol{\Delta}_{z}(\tau_{k+1}, \mathbf{0}, \boldsymbol{\beta}) - \boldsymbol{\Delta}_{z}(\tau_{k+1}, \mathbf{0}, \hat{\boldsymbol{\beta}}_{\pi})\|$$

$$+ \|\boldsymbol{\Delta}_{z}(\tau_{k+1}, \mathbf{0}, \hat{\boldsymbol{\beta}}_{\pi})\|,$$
(37)

where  $\tau_{k+1}$  ( $k \in \{1, 2, ...\}$ ) is the planned initial timing of the  $(k+1)^{th}$  walking step.

Suppose that the reference trajectories are generated to be compatible with the estimated reset map [29], we have  $\Delta_z(\tau_{k+1}, \mathbf{0}, \hat{\boldsymbol{\beta}}_{\pi}) = \mathbf{0}$ .

Because the reset map  $\Delta_z$  is continuously differentiable in t,  $\mathbf{x}$ , and  $\boldsymbol{\beta}$ , there exists a positive number  $r_1$  such that  $\Delta_z$  is Lipschitz continuous in these variables for any  $\mathbf{x}(0) \in B_{r_1}(\mathbf{0})$ . Thus, the approximation of  $\|\mathbf{z}\|_{k+1}^+$  becomes:

$$\|\mathbf{z}|_{k+1}^{+}\| = \|\mathbf{\Delta}_{z}(T_{k+1}, \mathbf{x}|_{k+1}^{-}, \boldsymbol{\beta})\|$$

$$\leq L_{T}|T_{k+1} - \tau_{k+1}| + L_{x}\|\mathbf{x}|_{k+1}^{-}\| + L_{\beta}\|\boldsymbol{\beta} - \hat{\boldsymbol{\beta}}_{\pi}\|,$$
(38)

where the positive numbers  $L_T$ ,  $L_x$ , and  $L_{\beta}$  are Lipschitz constants.

From Eq. (19),

$$\|\boldsymbol{\beta} - \hat{\boldsymbol{\beta}}_{\pi}\| = \|\tilde{\boldsymbol{\beta}}_{\pi}\| \le \beta_{M}. \tag{39}$$

As  $\mathbf{h}(-h_s \frac{\boldsymbol{\xi}}{\|\boldsymbol{\xi}\|})$  and  $\mathbf{Y}\hat{\boldsymbol{\beta}}_{\pi}$  are continuous functions of t,  $\mathbf{x}$ , and  $\hat{\boldsymbol{\beta}}_{\pi}$ , there exist positive numbers  $k_T$  and  $r_2$  such that

$$|T_{k+1} - \tau_{k+1}| \le k_T \|\mathbf{x}\|_{k+1}^- \| \tag{40}$$

for any  $\mathbf{x}(0) \in B_{r_2}(\mathbf{0})$  [45]. Note that the Zeno behavior associated with hybrid dynamical systems are excluded from the system in this study because of our focus on the local stability of the desired trajectories.

Thus, Eqs. (38)-(40) yield

$$\|\mathbf{z}\|_{k+1}^{+}\| \le (L_T k_T + L_x) \|\mathbf{x}\|_{k+1}^{-}\| + L_\beta \beta_M.$$
 (41)

Then,

$$\|\mathbf{z}\|_{k+1}^{+}\|^{2} \le L_{\Delta x} \|\mathbf{x}\|_{k+1}^{-}\|^{2} + 2L_{\beta}^{2}\beta_{M}^{2},$$
 (42)

where  $L_{\Delta x} := 2(L_T k_T + L_x)^2$ . Note that  $V_{\xi}|_{k+1}^+ = 0$  because  $\xi|_{k+1}^+ = 0$ . Thus, Eqs. (25), (27), (29), and (42) give

$$|V_t|_{k+1}^+ \le \frac{k_{t2}L_{\Delta x}}{k_{t1}} V_t|_{k+1}^- + 2k_{t2}L_{\beta}^2 \beta_M^2. \tag{43}$$

Evolution of  $V_t$  during the overall hybrid process. From Eq. (35),

$$|V_t|_{k+1}^- \le \int_{T_k}^{T_{k+1}} e^{-k_{f3}(T_{k+1}-v)} \varepsilon(v) dv + e^{-k_{f3}(T_{k+1}-T_k)} V_t|_k^+.$$
(44)

Then,

$$\begin{aligned} |V_{t}|_{k+1}^{+} &\leq \frac{k_{t2}L_{\Delta x}}{k_{t1}} e^{-k_{t3}(T_{k+1} - T_{k})} V_{t}|_{k}^{+} \\ &+ \frac{k_{t2}L_{\Delta x}}{k_{t1}} \int_{T_{k}}^{T_{k+1}} e^{-k_{t3}(T_{k+1} - v)} \varepsilon(v) dv \\ &+ 2k_{t2}L_{\beta}^{2} \beta_{M}^{2}. \end{aligned}$$
(45)

Recall that  $\varepsilon(t)$  is a known, bounded positive function on t > 0. Then, there exists a positive number  $\varepsilon_{\text{max}}$  such that the following inequality holds for all t:

$$\varepsilon(t) < \varepsilon_{\text{max}}.$$
 (46)

Thus,

$$\int_{T_k}^{T_{k+1}} e^{-k_{t3}(T_{k+1}-v)} \varepsilon(v) dv \le \frac{\varepsilon_{\max}}{k_{t3}} (1 - e^{-k_{t3}\Delta T_k}), \quad (47)$$

where  $\Delta T_k := T_{k+1} - T_k$  is the duration of the  $k^{th}$  walking step.

Combining Eqs. (45)-(47) yields

$$|V_t|_{k+1}^+ \le \delta_k V_t|_k^+ + b_k,$$
 (48)

where  $\delta_k:=\frac{k_{t2}L_{\Delta x}}{k_{t1}}e^{-k_{t3}\Delta T_k}$  and  $b_k:=2k_{t2}L_{\beta}^2\beta_M^2+\frac{k_{t2}L_{\Delta x}\varepsilon_{max}}{k_{t1}k_{t3}}(1-e^{-k_{t3}\Delta T_k}).$  From Eq. (40), we know that  $\Delta T_k$  is bounded. Hence, there

From Eq. (40), we know that  $\Delta T_k$  is bounded. Hence, there exist positive numbers  $\Delta T_{\min}$  and  $\Delta T_{\max}$  such that  $\Delta T_{\min} \leq \Delta T_k \leq \Delta T_{\max}$  holds for all  $k \in \{1, 2, ...\}$ . Then,

$$\delta_k \le \delta_{\text{max}} := \frac{k_{t2} L_{\Delta x}}{k_{t1}} e^{-k_{t3} \Delta T_{\text{min}}} \tag{49}$$

and

$$b_k \le b_{\text{max}} := 2k_{t2}L_{\beta}^2 \beta_M^2 + \frac{k_{t2}L_{\Delta x}\varepsilon_{\text{max}}}{k_{t1}k_{t3}} (1 - e^{-k_{t3}\Delta T_{\text{max}}}). \tag{50}$$

Since the continuous-phase convergence rate  $k_{t3}$  is sufficiently fast (i.e., condition (C6)), it can be chosen to satisfy

$$k_{t3} > \frac{1}{\Delta T_{\min}} ln(\frac{k_{t2} L_{\Delta x}}{k_{t1}}). \tag{51}$$

Then, from Eq. (49), we have

$$\delta_{\text{max}} < 1.$$
 (52)

Thus, for any  $k \in \{1, 2, ...\}$ , we have

$$|V_t|_{k+1}^+ \le \delta_{\max}^{k+1} V_t|_0^+ + \frac{1 - \delta_{\max}^{k+1}}{1 - \delta_{\max}} b_{\max}$$
 (53)

for any  $\mathbf{x}(0) \in B_r(\mathbf{0})$  with  $r = \min(r_{\xi}, r_1, r_2)$ . Therefore, when  $k \to \infty$ , i.e., when  $t \to \infty$ , we have

$$V_t|_{\infty}^+ \to \frac{b_{\text{max}}}{1 - \delta_{\text{max}}}.$$
 (54)

This inequality indicates the exponential convergence of  $\|\mathbf{x}\|$  to a bounded number during the overall hybrid process.

**Remark 4** (Satisfaction of the proposed stability condition (C5)). The condition (C5) can be met by properly choosing the matrices  $\mathbf{A}_c$ ,  $\mathbf{B}_c$ ,  $\mathbf{C}_c$ , and  $\mathbf{D}_c$  of the dynamic compensator in Eq. (21) such that  $\mathbf{A}_z = \begin{bmatrix} \mathbf{A}_c & \mathbf{B}_c \\ -\mathbf{C}_c & -\mathbf{D}_c \end{bmatrix}$  is Hurtwiz.

**Remark 5** (Satisfaction of the proposed stability condition (C6)). By the proof of Theorem 1, the condition (C6) is met if the continuous-phase convergence rate  $k_{t3}$  satisfies the inequality in Eq. (51). The rate can be assigned by properly choosing the control gains as explained below. From Eqs. (26), (33), and (36), we have  $k_{t3} = \min(\frac{\lambda_{\min}(\mathbf{Q}_z)}{\lambda_{\max}(\mathbf{P}_z)}, \frac{2\lambda_{\min}(\mathbf{K}_{\xi})}{k_M})$ , where  $\mathbf{P}_z$  can be obtained by solving the Lyapunov equation in Eq. (23) with  $\mathbf{Q}_z$  chosen as a symmetric positive definite matrix (e.g., an identity matrix),  $\mathbf{K}_{\xi}$  is a control gain, and  $k_M$  can be estimated based on joint limits and the expression of the inertia matrix  $\mathbf{M}$ .

**Remark 6** (Boundedness of parameter estimation error). Although the convergence of the parameter estimation error  $\tilde{\boldsymbol{\beta}}_{\pi}$  is not explicitly considered in the stability analysis, it is indeed bounded at the steady state because the parameter estimation by definition is bounded, as indicated by the conditions (C3) and (C4). In the following section, we will show that the parameter estimation error converges to zero in the absence of unmodeled uncertainties, i.e.,  $\tilde{\mathbf{f}} = \mathbf{0}$ , when certain conditions on the reference trajectory are met.

# 5 Parameter Estimation Convergence Analysis

This section derives the sufficient conditions under which the continuous ARC exponentially eliminates the parameter estimation error in the absence of the unmodeled uncertainties (i.e.,  $\tilde{\mathbf{f}} = \mathbf{0}$ ).

**Theorem 2.** Let the conditions (C5) and (C6) hold along with the following condition:

(C7) The reference trajectories satisfy the persistent excitation condition, i.e.,

$$\int_{t}^{t+T} \mathbf{Y}^{T}(\mathbf{q}_{d}, \dot{\mathbf{q}}_{d}, \dot{\mathbf{q}}_{d}, \ddot{\mathbf{q}}_{d}) \mathbf{Y}(\mathbf{q}_{d}, \dot{\mathbf{q}}_{d}, \dot{\mathbf{q}}_{d}, \ddot{\mathbf{q}}_{r}) d\nu \ge \varepsilon_{d} \mathbf{I}$$
(5)

for any  $t \ge t_0$ , where T,  $t_0$ , and  $\varepsilon_d$  are some positive numbers.

Then, in the absence of the unmodeled nonlinearity, i.e.,  $\tilde{\mathbf{f}} = \mathbf{0}$ , the proposed continuous-phase control law in Eq. (20) locally asymptotically stabilizes the hybrid system in Eq. (22) and drives the parameter estimation to the true value.

**Proof:** Let  $V_{\beta}$  be the Lyapunov function candidate associated with the parameter estimation error  $\tilde{\beta}$ .  $V_{\beta}$  is defined as [11]

$$V_{\beta}(\tilde{\boldsymbol{\beta}},\boldsymbol{\beta}) := \sum_{i=1}^{n_p} \int_0^{\tilde{\beta}_i} (\pi_i(\beta_i + \nu) - \beta_i) d\nu, \tag{56}$$

where  $\pi_i$  and  $\beta_i$  ( $i \in \{1, 2, ..., n_p\}$ ) are the  $i^{th}$  element of the function  $\pi$  and the vector  $\boldsymbol{\beta}$ , respectively.

From the parameter adaptation law in Eq. (16) and the definition of  $V_{\beta}$ , we obtain the first derivative of  $V_{\beta}$  as

$$\dot{V}_{\beta}(\tilde{\boldsymbol{\beta}},\boldsymbol{\beta}) = -\boldsymbol{\xi}^T \mathbf{Y} \tilde{\boldsymbol{\beta}}_{\pi}.$$
 (57)

In order to analyze the convergence of the parameter estimation error  $\tilde{\pmb{\beta}}_{\pi}$ , we introduce an augmented state

$$\tilde{\mathbf{x}} := \begin{bmatrix} \mathbf{x} \\ \tilde{\boldsymbol{\beta}} \end{bmatrix}, \tag{58}$$

along with an updated total Lyapunov function candidate

$$\tilde{V}_t(\tilde{\mathbf{x}}) = V_t(\mathbf{x}) + V_B(\tilde{\boldsymbol{\beta}}, \boldsymbol{\beta}). \tag{59}$$

The norm of  $\|\tilde{\mathbf{x}}\|$  is defined as  $\|\tilde{\mathbf{x}}\| := \sqrt{\|\mathbf{x}\|^2 + \|\tilde{\boldsymbol{\beta}}\|^2}$ . The overall hybrid closed-loop system associated with the augmented state is then:

$$\begin{cases} \begin{cases} \mathbf{M}\dot{\boldsymbol{\xi}} + (\mathbf{C} + \mathbf{K}_{\boldsymbol{\xi}})\boldsymbol{\xi} = \mathbf{h}(-h_{s}\frac{\boldsymbol{\xi}}{\|\boldsymbol{\xi}\|}) + \mathbf{Y}\tilde{\boldsymbol{\beta}}_{\pi} - \tilde{\mathbf{f}} \\ \dot{\boldsymbol{z}} = \mathbf{A}_{z}\mathbf{z} + \mathbf{B}_{z}\boldsymbol{\xi} & \text{if } (t, \mathbf{x}^{-}) \notin S_{x}; \\ \dot{\boldsymbol{\beta}} = -\Gamma\boldsymbol{\tau} \\ \begin{bmatrix} \boldsymbol{\xi}^{+} \\ \mathbf{z}^{+} \\ \tilde{\boldsymbol{\beta}}^{+} \end{bmatrix} = \begin{bmatrix} \mathbf{0} \\ \mathbf{\Delta}_{z} \\ \tilde{\boldsymbol{\beta}}^{-} \end{bmatrix} & \text{if } (t, \mathbf{x}^{-}) \in S_{x}. \end{cases}$$

$$(60)$$

Evolution of  $\tilde{V}_t$  during continuous phases. Combining the derivatives of the individual Lyapunov functions  $V_t$  and  $V_{\beta}$  in Section 4 and given that  $\tilde{\mathbf{f}} = \mathbf{0}$ , we have

$$\dot{\tilde{V}}_{t} = \dot{V}_{t} + \dot{V}_{\beta}$$

$$= \boldsymbol{\xi}^{T} (\mathbf{Y} \tilde{\boldsymbol{\beta}}_{\pi} - \mathbf{K}_{\xi} \boldsymbol{\xi} + \mathbf{h}(-h_{s} \frac{\boldsymbol{\xi}}{\|\boldsymbol{\xi}\|})) - \mathbf{z}^{T} \mathbf{Q}_{z} \mathbf{z} - \boldsymbol{\xi}^{T} \mathbf{Y} \tilde{\boldsymbol{\beta}}_{\pi}.$$
(61)

From the condition (C1), the above equation becomes

$$\dot{\tilde{V}}_t \le -\boldsymbol{\xi}^T \mathbf{K}_{\boldsymbol{\xi}} \boldsymbol{\xi} - \mathbf{z}^T \mathbf{Q}_z \mathbf{z}. \tag{62}$$

Recall  $T_k$  ( $k \in \{1,2,...\}$ ) is the initial moment of the  $k^{th}$  walking step. Let  $(\bar{\mathbf{x}}, \tilde{\boldsymbol{\beta}})$  be the solution to the continuous-phase subsystem of Eq. (60) on  $t > T_k$  with initial condition  $[\bar{\mathbf{x}}^T(T_k^+), \bar{\boldsymbol{\beta}}^T(T_k^+)]^T = \tilde{\mathbf{x}}(T_k^+)$ . Then,  $[\bar{\mathbf{x}}^T, \bar{\boldsymbol{\beta}}^T]^T = \tilde{\mathbf{x}}$  on  $t \in (T_k, T_{k+1}]$ .

The inequality in Eq. (62) implies that  $\bar{\mathbf{x}} \in L_2 \cap L_\infty$  and  $\bar{\boldsymbol{\beta}} \in L_\infty$ . From the continuous-phase subsystem of Eq. (60),  $\dot{\mathbf{x}} \in L_\infty$ . Thus,  $\bar{\mathbf{x}}$  is uniformly continuous. Also, for  $\bar{\mathbf{x}}$  and  $\bar{\boldsymbol{\beta}}$ , all terms of the continuous-phase subsystem are uniformly continuous, and thus  $\dot{\bar{\mathbf{x}}}$  is uniformly continuous. Then, by Barbalat's lemma [4],  $\bar{\mathbf{x}} \to \mathbf{0}$  locally exponentially on  $t > T_k$ . Accordingly,  $\mathbf{x}$  locally exponentially diminishes on  $t \in (T_k, T_{k+1}]$ . Thus, from the continuous-phase subsystem of Eq. (60),  $\mathbf{Y}\bar{\boldsymbol{\beta}}_\pi$  locally exponentially approaches zero on  $t \in (T_k, T_{k+1}]$ . If the reference trajectories satisfy the persistent excitation condition (i.e., the condition (C7)), then the parameter estimation error  $\tilde{\boldsymbol{\beta}}_\pi$  exponentially diminishes on  $t \in (T_k, T_{k+1}]$  [4].

Hence, there exist positive numbers  $\tilde{k}_t$ ,  $\tilde{\alpha}_t$ , and  $\tilde{r}_{t1}$  such that the augmented state  $\tilde{\mathbf{x}}$  satisfies [30]

$$\|\tilde{\mathbf{x}}(t)\| \le \tilde{k}_t e^{\tilde{\alpha}_t(t-T_k)} \|\tilde{\mathbf{x}}\|_k^+ \|$$
(63)

for any  $\tilde{\mathbf{x}}(0) \in B_{\tilde{r}_{t1}}(\mathbf{0})$  and  $t \in (T_k, T_{k+1}], k \in \{1, 2, ...\}$ ; that is, the augmented state  $\tilde{\mathbf{x}}$ , including the parameter estimation error  $\tilde{\boldsymbol{\beta}}_{\pi}$ , exponentially diminishes during continuous phases.

**Evolution of**  $\tilde{V}_t$  across jumps. By the definition of the Lyapunov function  $V_{\beta}$  in Eq. (56), the discrete event of state-triggered jumps does not cause a sudden change in  $V_{\beta}$ .

Therefore,  $\tilde{\boldsymbol{\beta}}^+ = \tilde{\boldsymbol{\beta}}^-$ , and accordingly  $\tilde{\boldsymbol{\beta}}_{\pi}^+ = \tilde{\boldsymbol{\beta}}_{\pi}^-$ .

The approximation of  $\|\mathbf{z}^+\|$  right after an impact at t =

 $T_{K+1}$  becomes

$$\|\mathbf{z}|_{k+1}^{+}\| = \|\mathbf{\Delta}_{z}(T_{k+1}, \mathbf{x}|_{k+1}^{-}, \boldsymbol{\beta})\|$$

$$\leq \|\mathbf{\Delta}_{z}(T_{k+1}, \mathbf{x}|_{k+1}^{-}, \boldsymbol{\beta}) - \mathbf{\Delta}_{z}(\tau_{k+1}, \mathbf{x}|_{k+1}^{-}, \boldsymbol{\beta})\|$$

$$+ \|\mathbf{\Delta}_{z}(\tau_{k+1}, \mathbf{x}|_{k+1}^{-}, \boldsymbol{\beta}) - \mathbf{\Delta}_{z}(\tau_{k+1}, \mathbf{0}, \boldsymbol{\beta})\|$$

$$+ \|\mathbf{\Delta}_{z}(\tau_{k+1}, \mathbf{0}, \boldsymbol{\beta}) - \mathbf{\Delta}_{z}(\tau_{k+1}, \mathbf{0}, \hat{\boldsymbol{\beta}}_{\pi})\|$$

$$+ \|\mathbf{\Delta}_{z}(\tau_{k+1}, \mathbf{0}, \hat{\boldsymbol{\beta}}_{\pi})\|.$$
(64)

Then, following similar derivations as in Section 4 and noting that  $\|\tilde{\boldsymbol{\beta}}_{\pi}\| \leq \|\tilde{\boldsymbol{\beta}}\|$ , there exist a positive number  $\tilde{r}_{t2}$  such that

$$\|\mathbf{z}|_{k+1}^{+}\| \le (L_T k_T + L_x) \|\mathbf{x}|_{k+1}^{-}\| + L_{\beta} \|\tilde{\boldsymbol{\beta}}\|$$
 (65)

for any  $\tilde{\mathbf{x}}(0) \in B_{\tilde{r}_{t2}}(\mathbf{0})$  and  $t \in (T_k, T_{k+1}], k \in \{1, 2, ...\}$ . Correspondingly,

$$\|\mathbf{z}|_{k+1}^{+}\|^{2} \le 2(L_{T}k_{T} + L_{x})^{2}\|\mathbf{x}|_{k+1}^{-}\|^{2} + 2L_{\beta}^{2}\|\tilde{\boldsymbol{\beta}}\|^{2}.$$
 (66)

Since 
$$\tilde{\boldsymbol{\beta}}|_{k+1}^+ = \tilde{\boldsymbol{\beta}}|_{k+1}^-$$
 and  $\boldsymbol{\xi}|_{k+1}^+ = \boldsymbol{\xi}|_{k+1}^-$ , we have

$$\|\tilde{\mathbf{x}}\|_{k+1}^{+}\|^{2} = \|\mathbf{z}\|_{k+1}^{+}\|^{2} + \|\boldsymbol{\xi}\|_{k+1}^{+}\|^{2} + \|\tilde{\boldsymbol{\beta}}\|^{2}$$

$$\leq 2(L_{T}k_{T} + L_{x})^{2}\|\mathbf{x}\|_{k+1}^{-}\|^{2} + (2L_{\beta}^{2} + 1)\|\tilde{\boldsymbol{\beta}}\|^{2} \quad (67)$$

$$\leq \tilde{L}_{x}^{2}\|\tilde{\mathbf{x}}\|_{k+1}^{-}\|^{2},$$

where 
$$\tilde{L}_x := \max(\sqrt{2(L_Tk_T + L_x)^2}, \sqrt{2L_\beta^2 + 1})$$
.

Evolution of  $\tilde{V}_t$  during the overall hybrid process. Combining the evolution of the augmented state  $\tilde{\mathbf{x}}$  during the continuous phase and across the state-triggered jump yields

$$\|\tilde{\mathbf{x}}\|_{k+1}^{+}\| \le \tilde{L}_{x}\|\tilde{\mathbf{x}}\|_{k+1}^{-}\| \le \tilde{L}_{x}\tilde{k}_{t}e^{-\tilde{\alpha}_{t}\Delta T_{k}}\|\tilde{\mathbf{x}}\|_{k}^{+}\|$$
 (68)

for any  $\tilde{\mathbf{x}}(0) \in B_{\tilde{r}}(\mathbf{0})$  with  $\tilde{r} := \min(r, \tilde{r}_{t1}, \tilde{r}_{t2})$ . Therefore, if the control gains are chosen such that

$$L_{\tilde{x}}\tilde{k}_t e^{-\tilde{\alpha}_t \Delta T_k} < 1$$
,

then for any  $\tilde{\mathbf{x}}(0) \in B_{\tilde{r}}(\mathbf{0})$  the augmented state  $\tilde{\mathbf{x}}$  will exponentially converge to zero for the overall hybrid dynamical process. Accordingly, the parameter estimation error  $\tilde{\boldsymbol{\beta}}$  will also exponentially converge to zero.

**Remark 7** (Satisfaction of the persistent excitation condition (C7)). By Theorem 2, to realize accurate parameter estimation requires that the reference trajectory  $\mathbf{q}_d(t)$  should satisfy the persistent excitation condition (C7). Because walking on flat horizontal terrain is typically periodic,  $\mathbf{q}_d(t)$  is typically planned as periodic [46]. Then, the condition is satisfied if

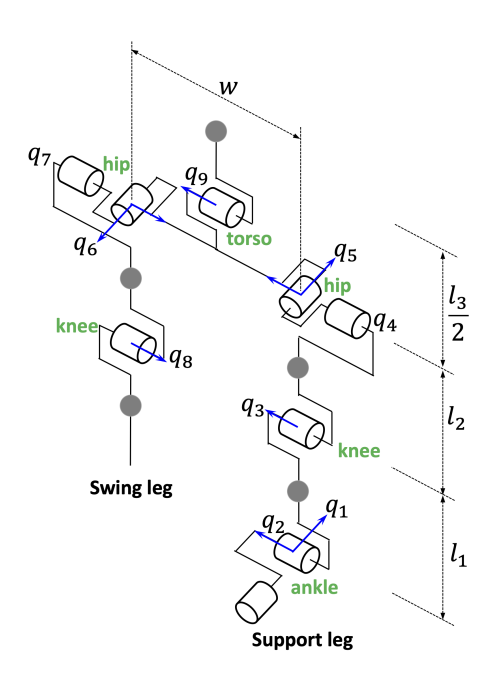


Fig. 3. A 3-D biped with nine revolute joints [35]

the sampling increment of controller discretization in realworld implementation is significantly smaller than the walking period [4], which can easily be met as the sampling rate in practical applications is typically about 1 ms whereas the walking period is about 0.3 - 1.5 s.

## 6 Simulation Results

This section presents simulation results that demonstrate the effectiveness of the proposed trajectory tracking control method in realizing stable 3-D bipedal robotic walking in the presence of parametric and unmodeled uncertainties.

#### **6.1** Simulation Setup

The robot model [47] considered in this study is shown in Fig. 3. The robot has nine revolute joints with the mass of each link lumped at the link's center. Physical parameters of the simulated robot model are given in Tab. 1.

Table 1. Robot Model Parameters		
parameter	variable	value
lower-limb mass	$m_1$	0.4  kg
upper-limb mass	$m_2$	0.8  kg
torso mass	$m_T$	4.8 kg
lower-limb length	$l_1$	0.4 m
upper-limb length	$l_2$	0.4 m
torso length	$l_3$	0.4 m
hip width	w	0.3 m

To stabilize the closed-loop system and achieve a reliable tracking performance, the following controller parameters should be properly tuned:

- (a) The gain of the linear stabilizing feedback term,  $\mathbf{K}_{\xi}$ .
- (b) The gain of the parameter adaptation law,  $\Gamma$ .
- (c) The parameters of the robust controller, including the matrices of the dynamic compensator (i.e.,  $\mathbf{A}_c$ ,  $\mathbf{B}_c$ ,  $\mathbf{C}_c$ , and  $\mathbf{D}_c$ ) and the parameters of the SMC (i.e.,  $\mathbf{K}_s$ ,  $\phi$ ,  $\varepsilon_1$ , and  $\varepsilon_2$ ).

As indicated by the stability and performance analysis in Sections 4 and 5, the general rules for tuning these controller parameters include:

- (a) A larger  $\mathbf{K}_{\xi}$  generally increases the rate of continuous-phase convergence of the tracking error (i.e.,  $k_{t3}$ ).
- (b) A larger  $\Gamma$  can result in faster continuous-phase convergence of the estimated parameters to their true values.
- (c) Faster poles of the transfer function from  $\boldsymbol{\xi}$  to  $\mathbf{e}$  (i.e.,  $(s\mathbf{I}_{n\times n} + \mathbf{G}_c(s))^{-1}$ ) can lead to faster continuous-phase convergence of the tracking error.
- (d) A smaller  $\phi$ , a lager  $\varepsilon_1$ , or a smaller  $\varepsilon_2$  can all expand the range of states that the ideal SMC (i.e.,  $-h_s \frac{\xi}{\|\xi\|}$ ) acts on.

# 6.2 Performance Comparison under Parametric and Unmodeled Uncertainties

To validate the effectiveness of the proposed continuous ARC in achieving the control objective as stated in Section 3, four different controllers were implemented and compared: (a) the proposed ARC, (b) a robust controller, (c) an adaptive controller, and (d) a baseline controller without robust feedback or parameter adaptation, which is equivalent to our previous input-output linearizing controller [32–35].

For the purpose of performance comparison, the following values of uncertainties and initial conditions are used in the simulations of all four controllers:

- (a) The maximum norm of the unmodeled uncertainty is 30, i.e.,  $h_f = 30$ .
- (b) The initial position and velocity tracking errors of each joint are 0.2 rad (about 11°) and 0.3 rad/s (about 17°/s), respectively. Relatively large initial tracking errors are chosen here so as to test the regions of attraction of the controllers.
- (c) The unknown parameters are the robot's link masses, i.e.,  $\boldsymbol{\beta} = [m_1 \ m_2 \ m_T]^T = [0.4 \ 0.8 \ 4.8]^T \text{ kg.}$
- (d) The lower and the upper bounds of the parameter estimation are set as  $\boldsymbol{\beta}_{\min} = [-1.1 0.4 1.2]^T$  kg and  $\boldsymbol{\beta}_{\max} = [3.4 \ 2.3 \ 16.8]$  kg, respectively. This setting allows us to assess the performance of the proposed ARC under relatively large bounds of parameter estimation.
- (e) The initial parameter estimation is  $\hat{\boldsymbol{\beta}}(0) = \hat{\boldsymbol{\beta}}_{\pi}(0) = [2.7 \ 2.1 \ 10.8]^T$  kg, corresponding to an initial estimation error of  $\tilde{\boldsymbol{\beta}}(0) = \tilde{\boldsymbol{\beta}}_{\pi}(0) = [2.3 \ 1.3 \ 6]^T$  kg. These significant initial parametric uncertainties permit a clear comparison in parameter estimation accuracy as well as robustness.

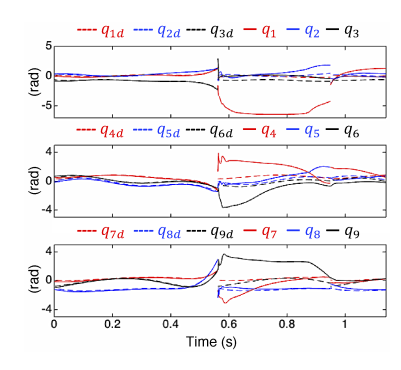


Fig. 4. Trajectory tracking results of Baseline Control (Case 1) during three simulated walking steps

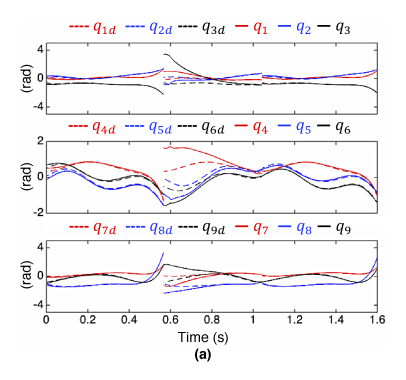


Fig. 5. Tracking results of Adaptive Control (Case 2) during three simulated walking steps

The parameters of the four controllers are chosen as:

Case 1: Baseline Control (BC): The control law is formed as in Section 3 with the adaptive and robust gains turned off. Specifically, the control gains are chosen as:  $\mathbf{A}_c = \mathbf{B}_c = \mathbf{C}_c = \mathbf{0}_{9\times 9}$  with  $\mathbf{0}_{9\times 9} \in \mathbb{R}^{9\times 9}$ ;  $\mathbf{D}_c = \omega_c \mathbf{I}_{9\times 9}$  ( $\omega_c = 40 \text{ rad/s}$ );  $\phi = 0$ ;  $\mathbf{\Gamma} = \mathbf{0}_{3\times 3}$ ; and  $\mathbf{K}_{\xi} = 30\mathbf{I}_{9\times 9}$ . Using these parameters renders a corner frequency for the sliding mode as  $\omega_c = 40 \text{ rad/s}$  and an effective stabilizing feedback gain for  $\boldsymbol{\xi}$  as  $\mathbf{K}_{\xi} + \omega_c \mathbf{I}_{9\times 9} = 70\mathbf{I}_{9\times 9}$ . The position trajectory tracking results are shown in Fig. 4. The poor trajectory tracking performance indicates that the robot fails to sustain walking within three steps.

Case 2: Adaptive Control (AC): The control law is formed as in Section 3 with the robust gains turned off. The values of the control gains are chosen to be the same as in Case 1 except for the parameter adaptation gain,  $\Gamma$ , which is chosen as  $\Gamma = 40 I_{3 \times 3}$ . The position trajectory tracking results are shown in Fig. 5. The parameter estimation and torque profile are omitted due to the overly large overshoot of the responses.

Case 3: Robust Control (RC): The control law is formed as in Section 3 with the parameter adaptation turned off. The dynamic compensator is set as:  $\mathbf{A}_c = \mathbf{0}_{9\times 9}$ ,  $\mathbf{B}_c = 100\mathbf{I}_{9\times 9}$ ,  $\mathbf{C}_c = \mathbf{I}_{9\times 9}$ , and  $\mathbf{D}_c = 2\omega_c\mathbf{I}_{9\times 9}$  ( $\omega_c = 10$ ), which render the corner frequency of the sliding mode

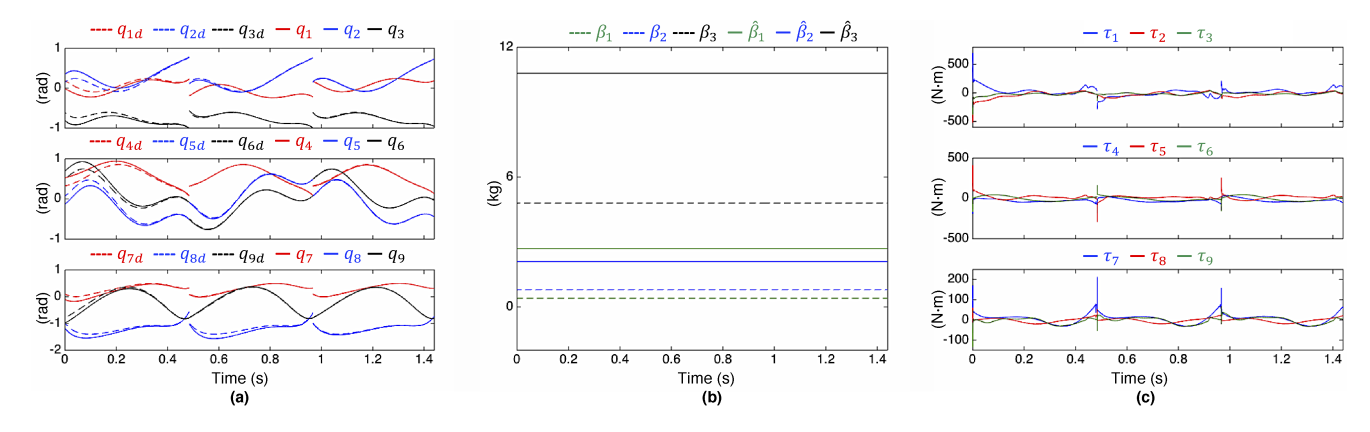


Fig. 6. Tracking results of Robust Control (Case 3) during three simulated walking steps. a) Joint position tracking. b) Parameter estimation. c) Joint torque profiles.

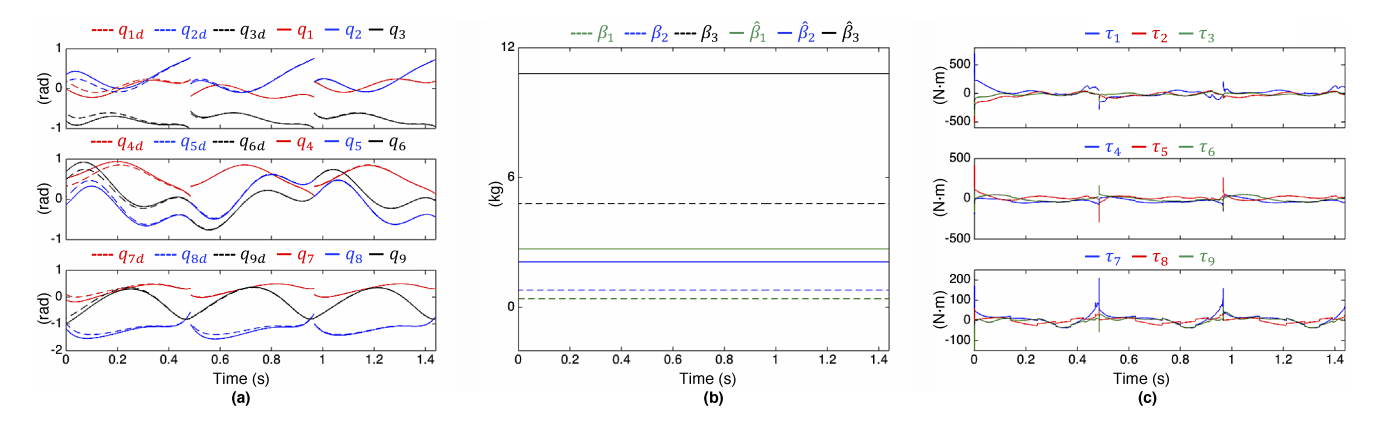


Fig. 7. Tracking results of Robust Control in the presence of unmodeled nonlinearities different from Case 3. a) Joint position tracking. b) Parameter estimation. c) Joint torque profiles.

as  $\omega_c = 10$ . The parameters of the SMC are chosen as:  $\phi = 30$ ,  $\varepsilon_1 = 1$ , and  $\varepsilon_2 = 0.5$ . The adaptation law is turned off by choosing  $\Gamma = \mathbf{0}_{3\times3}$ . The linear stabilizing feedback gains for  $\boldsymbol{\xi}$  are chosen as  $\mathbf{K}_{\boldsymbol{\xi}} = 40\mathbf{I}_{9\times9}$  and  $\mathbf{K}_s = 20\mathbf{I}_{9\times9}$ . These gains produce an overall feedback gain for  $\boldsymbol{\xi}$  as  $\mathbf{K}_{\boldsymbol{\xi}} + \mathbf{K}_s = 60\mathbf{I}_{9\times9}$ . Note that both the corner frequency and overall feedback gain are smaller than those of the BC and the AC. The simulation results are shown in Fig. 6.

Case 4: Adaptive Robust Control (ARC): The control law is formed as in Section 3 with both robust and adaptive control action turned on. The feedback gains, the dynamic compensator, and the SMC are set exactly the same as the RC. The only gain different from the RC is the adaptation gain, which is chosen the same as the AC, i.e.,  $\Gamma = 40I_{3\times3}$ . The simulation results are shown in Fig. 8.

# **6.3** Discussions on Performance Comparison

Based on the simulation results, the performance of the four controllers are compared and discussed as follows:

**Final tracking error and convergence rate:** To assess and compare the transient performance and final accuracy of trajectory tracking, we evaluate the rate of the actual tra-

jectory's convergence to the reference trajectory along with the tracking error near steady state. The BC and the AC both have an effective feedback gain and a corner frequency larger than those of the RC and ARC. However, under the relatively large uncertainties and initial tracking errors, the BC is not able to stabilize the hybrid system as shown in Fig. 4, and the AC causes a very large transient parameter estimation error that induces an overly large control effort. In contrast, thanks to the robust feedback term, the RC and the ARC realizes higher final tracking accuracy and faster convergence rate under unmodeled uncertainties, as shown in Figs. 6 (a) and 8 (a).

Control effort demanded: Simulation results show that AC, RC, and ARC demand different levels of control effort for stabilization. The BC is not included in the comparison as it fails to stabilize the system. The torque profile under the AC is not shown due to the overly large overshoot, which is induced by the rejection of the large parameter estimation error under unmodeled uncertainties. However, as shown in Figs. 6 (c) and 8 (c), the RC and the ARC demand relatively low peak torque. The comparison highlights the necessity of enforcing a finite bound to the parameter estimation produced by the adaptation law in Eq. (16), which is missing in the de-

sign of AC.

Control chattering: Due to the use of aggressive nonlinear robust feedback, i.e., the modified SMC, the RC and the ARC are subject to certain amount of control chattering, especially at the initial period of each walking step (see Figs. 6 (c) and 8 (c)). During these initial periods, the ideal SMC is activated to reject the tracking error divergence caused by the uncontrolled state-triggered jumps upon foot-landing events. However, as confirmed through simulations, the ARC causes less chattering than the DC thanks to the incorporation of parameter estimation.

Robustness: To evaluate the robustness of the RC and the ARC under relatively aggressive disturbances, the nonlinear function  $\tilde{\mathbf{f}}$  is modified to include an additional term,  $10 \cdot (-1)^{\frac{t}{0.2}}$ , which emulates a relatively large disturbance that instantaneously switches signs at least twice during a walking step. Simulation results are shown in Figs. 7 and 9. As shown in the figures, the tracking performances of both controllers are close to the cases where the additional nonlinear function term is absent (i.e., Figs. 6 and 8), which illustrates the robustness of the RC and the ARC in rejecting unmodeled uncertainties. Because unknown external payloads are an important source of uncertainties for real-world applications of legged locomotion, the robustness of ARC is further assessed under parametric uncertainty only in the torso mass  $\beta_3$  in addition to the unmodeled nonlinearity  $\tilde{\mathbf{f}}$  as specified in Section 6.2. The initial torso mass estimation error  $\tilde{\beta}_3(0)$  is set as 8 kg, which is 167% of the true value of  $\beta_3$ . Despite the significant initial uncertainty in the torso mass, the proposed ARC realizes accurate trajectory tracking and parameter estimation with a relatively fast convergence rate, as shown in Fig. 11.

Parameter estimation convergence: The simulation results show that both the AC and the ARC drive the parameter estimations to a close neighborhood of their true values. However, the estimation error under the AC increases to an overly large value before converging towards zero, causing overly large joint torques. Thus, the parameter estimation plot of the AC is omitted. In contrast, the ARC achieves a small estimation error without causing an overly large joint torque thanks to the smooth projection of parameter estimation, as shown in Fig. 8 (c).

#### Parameter estimation without unmodeled uncertainties:

As predicted by Theorem 2, the ARC should be able to eliminate parameter estimation errors when the unmodeled uncertainties are absent (i.e.,  $\tilde{\mathbf{f}} = \mathbf{0}$ ). The control parameters and the simulation setup are chosen exactly the same as in Section 6.1, except that the unmodeled uncertainties are set as  $\tilde{\mathbf{f}} = \mathbf{0}$ . As shown in Fig. 10, the ARC indeed eliminates the parameter estimation error at the steady state, which validates Theorem 2.

#### 7 Discussions

The proposed control approach can be potentially extended and applied to realize nonperiodic legged locomotion. The desired gait is chosen as periodic time trajectories in this study mainly for simplifying the motion planning task. Specifically, such desired trajectories provably satisfy the persistent excitation condition (i.e., the condition (C7)) that is demanded to achieve accurate parameter estimation, as explained in Remark 7. Yet, the theoretical basis of the proposed approach (i.e., the Lyapunov-based closed-loop stability analysis shown in the proofs of the main theorems) does not necessarily assume the periodicity of the desired gait. To extend the proposed approach to realize nonperiodic legged locomotion, we will integrate the approach with nonperiodic motion planning [48] by deriving conditions under which nonperiodic trajectories meet the persistent excitation condition.

One limitation of the proposed control approach in handling real-world legged locomotion is that it does not explicitly respect the feasibility of the ground reaction force and center of pressure. Particularly, in the presence of overly large uncertainties, the robust feedback term (e.g., the SMC) of the proposed control approach may induce chattering that violates ground-contact constraints such as unilateral and friction-cone constraints, which can cause the loss of proper contact between the support foot and the ground and may even lead to falling. To overcome this limitation, we will investigate the integration of the proposed approach with real-time optimization so as to realize satisfactory trajectory tracking simultaneously with the guaranteed feasibility for the ground-contact constraints. This potential integration seems promising as indicated by recent progress in combining quadratic programming based real-time optimization and feedback control such as input-output linearizing control [49] and control barrier functions [50].

Another limitation of the proposed control approach lies in that it only addresses fully actuated bipedal walking instead of the general multi-domain walking [51], which comprises domains of full actuation, underactuation, and over actuation. In our future work, we will integrate the proposed controller design with our previous work on tracking control of multi-domain hybrid systems [52] to enable stable multi-domain walking even under uncertainties.

# 8 Conclusions

A continuous adaptive robust control law has been proposed for hybrid systems with state-triggered jumps to achieve accurate trajectory tracking of fully actuated 3-D bipedal walking under parametric uncertainties and unmodeled disturbances. The control law was derived based on the incorporation of the construction of multiple Lyapunov functions into the control Lyapunov function. Specifically, the stability, tracking performance, and parameter estimation convergence of the closed-loop hybrid system were analyzed by explicitly examining the effects of state-triggered jumps on the evolution of the Lyapunov function under uncertainties. These analyses produced sufficient conditions

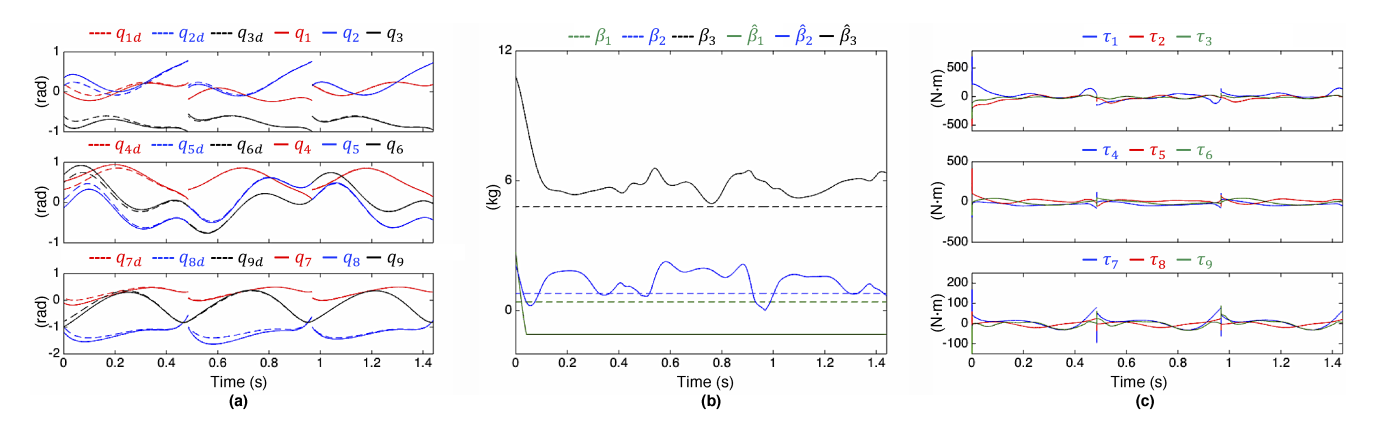


Fig. 8. Tracking results of Adaptive Robust Control (Case 4) during three simulated walking steps. a) Joint position tracking. b) Parameter estimation. c) Joint torque profiles.

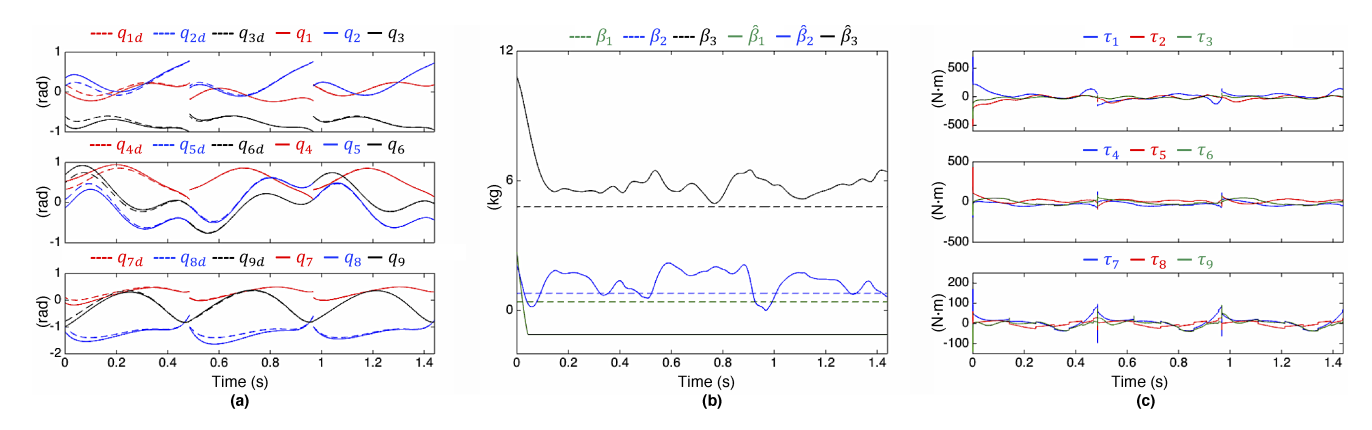


Fig. 9. Tracking results of Adaptive Robust Control in the presence of unmodeled nonlinearities different from Case 4. a) Joint position tracking. b) Parameter estimation. c) Joint torque profiles.

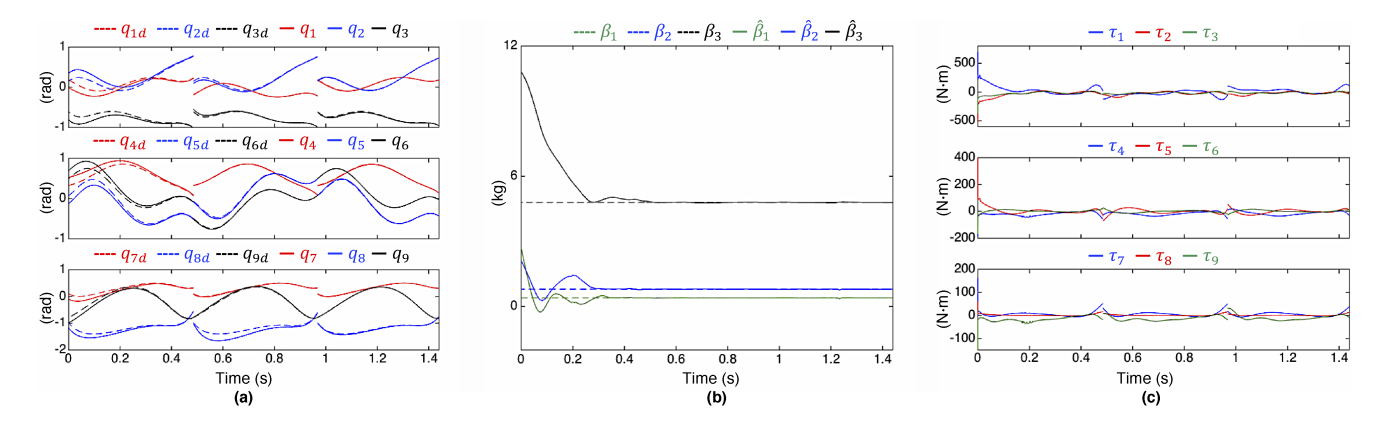


Fig. 10. Tracking results of Adaptive Robust Control in the absence of unmodeled nonlinearities. a) Joint position tracking. b) Parameter estimation. c) Joint torque profiles.

that were then used to guide the design of a continuous ARC for ensuring the stability and performance of hybrid systems with state-triggered jumps that include fully actuated bipedal walking robots. Through simulated walking experiments in the presence of parametric and unmodeled uncertainties, the tracking performance of the proposed ARC and three other widely used controllers were assessed and compared. The simulation results demonstrated that the proposed ARC achieves accurate tracking and fast convergence

while demanding the least amount of control effort and inducing the least degree of chattering. Furthermore, additional simulation results showed that the proposed control law achieves asymptotic parameter estimation convergence under parametric uncertainties alone.

#### References

[1] Kolathaya, S., and Ames, A. D., 2014. "Exponential convergence of a unified clf controller for robotic

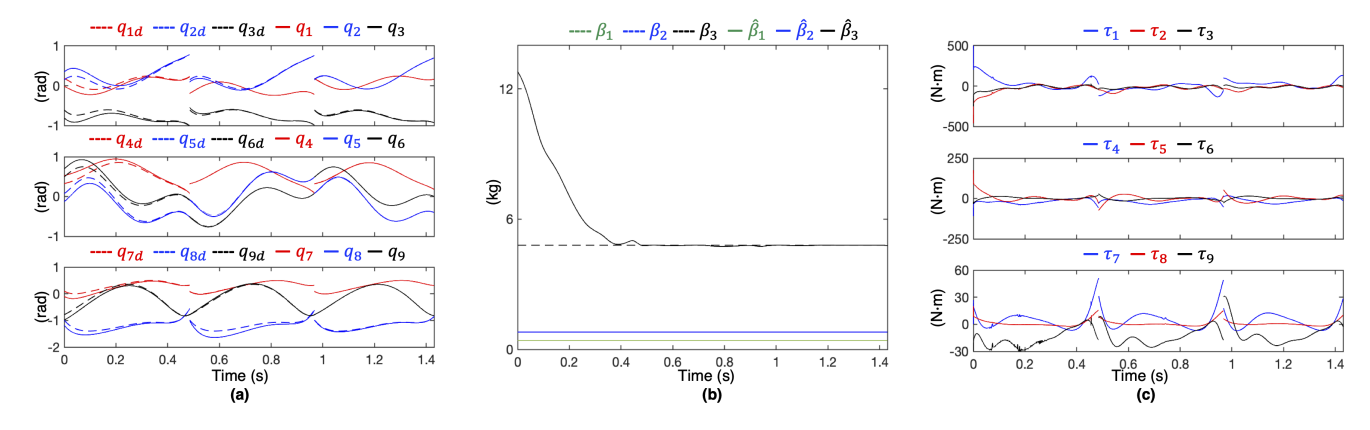


Fig. 11. Tracking results of Adaptive Robust Control in the presence of unmodeled nonlinearity (same as Case 4) and parametric uncertainty only in the torso mass  $\beta_3$ . a) Joint position tracking. b) Parameter estimation. c) Joint torque profiles. a) Joint position tracking. b) Parameter estimation. c) Joint torque profiles.

- systems under parameter uncertainty". In Proc. Amer. Contr. Conf., pp. 3710–3715.
- [2] Nguyen, Q., and Sreenath, K., 2015. "Optimal robust control for bipedal robots through control Lyapunov function based quadratic programs". In Proc. Robot.: Sc. Syst.
- [3] Yeatman, M., Lv, G., and Gregg, R. D., 2019. "Decentralized passivity-based control with a generalized energy storage function for robust biped locomotion". *ASME J. Dyn. Syst., Meas., Contr.*, **141**(10).
- [4] Slotine, J. J. E., and Li, W., 1991. *Applied nonlinear control*. Springer.
- [5] Krstic, M., Kokotovic, P. V., and Kanellakopoulos, I., 1995. *Nonlinear and adaptive control design*. John Wiley & Sons, Inc.
- [6] Sastry, S., and Bodson, M., 2011. *Adaptive control:* stability, convergence and robustness. Courier Corporation.
- [7] Yuan, C., 2017. "Distributed adaptive switching consensus control of heterogeneous multi-agent systems with switched leader dynamics". *Nonlinear Anal.: Hybrid Syst.*, **26**, pp. 274–283.
- [8] Zhou, K., and Doyle, J. C., 1998. *Essentials of robust control*, Vol. 104. Prentice Hall.
- [9] Skogestad, S., and Postlethwaite, I., 2007. *Multivariable feedback control: analysis and design*, Vol. 2. Wiley.
- [10] Yao, B., and Tomizuka, M., 1997. "Adaptive robust control of siso nonlinear systems in a semi-strict feedback form". *Automatica*, **33**(5), pp. 893–900.
- [11] Yao, B., and Tomizuka, M., 2001. "Adaptive robust control of mimo nonlinear systems in semi-strict feedback forms". *Automatica*, **37**(9), pp. 1305–1321.
- [12] Yao, B., Hu, C., and Wang, Q., 2011. "An orthogonal global task coordinate frame for contouring control of biaxial systems". *IEEE/ASME Trans. Mechatron.*, 17(4), pp. 622–634.
- [13] Liao, J., Chen, Z., and Yao, B., 2018. "Model-based coordinated control of four-wheel independently driven skid steer mobile robot with wheel–ground interaction

- and wheel dynamics". *IEEE Trans. Ind. Inf.*, **15**(3), pp. 1742–1752.
- [14] Chen, Z., Li, C., Yao, B., Yuan, M., and Yang, C., 2019. "Integrated coordinated/synchronized contouring control of a dual-linear-motor-driven gantry". *IEEE Trans. Ind. Electron.*, **67**(5), pp. 3944–3954.
- [15] Chen, Z., Huang, F., Yang, C., and Yao, B., 2019. "Adaptive fuzzy backstepping control for stable nonlinear bilateral teleoperation manipulators with enhanced transparency performance". *IEEE Trans. Ind. Electron.*, **67**(1), pp. 746–756.
- [16] Yuan, M., Chen, Z., Yao, B., and Liu, X., 2019. "Fast and accurate motion tracking of a linear motor system under kinematic and dynamic constraints: an integrated planning and control approach". *IEEE Trans. Contr. Syst. Tech.*, **29**(2), pp. 804–811.
- [17] Ilg, W., Albiez, J., Jedele, H., Berns, K., and Dillmann, R., 1999. "Adaptive periodic movement control for the four legged walking machine bisam". In Proc. IEEE Int. Conf. Robot. Autom., Vol. 3, pp. 2354–2359.
- [18] Fujimoto, Y., Obata, S., and Kawamura, A., 1998. "Robust biped walking with active interaction control between foot and ground". In Proc. IEEE Int. Conf. Robot. Autom., Vol. 3, pp. 2030–2035.
- [19] Raibert, M., Tzafestas, S., and Tzafestas, C., 1993. "Comparative simulation study of three control techniques applied to a biped robot". In Proc. IEEE Syst., Man, Cyber. Conf., Vol. 1, pp. 494–502.
- [20] Tzafestas, S., Raibert, M., and Tzafestas, C., 1996. "Robust sliding-mode control applied to a 5-link biped robot". *J. Intel. Robot. Syst.*, **15**(1), pp. 67–133.
- [21] Zohdy, M. A., and Zaher, A. A., 2000. "Robust control of biped robots". In Proc. Amer. Contr. Conf., Vol. 3, pp. 1473–1477.
- [22] Moosavian, S. A. A., Takhmar, A., and Alghooneh, M., 2007. "Regulated sliding mode control of a biped robot". In Proc. IEEE Int. Conf. Mechatron. Autom., pp. 1547–1552.
- [23] Golliday, C., and Hemami, H., 1977. "An approach to analyzing biped locomotion dynamics and design-

- ing robot locomotion controls". *IEEE Trans. Autom. Contr.*, **22**(6), pp. 963–972.
- [24] Goswami, A., Thuilot, B., and Espiau, B., 1998. "A study of the passive gait of a compass-like biped robot: Symmetry and chaos". *Int. J. Robot. Res.*, **17**(12), pp. 1282–1301.
- [25] Hiskens, I. A., 2001. "Stability of hybrid system limit cycles: Application to the compass gait biped robot". In Proc. IEEE Conf. Dec. Contr., Vol. 1, pp. 774–779.
- [26] Hamed, K., Safaee, B., and Gregg, R. D., 2019. "Dynamic output controllers for exponential stabilization of periodic orbits for multidomain hybrid models of robotic locomotion". *ASME J. Dyn. Syst.*, *Meas.*, *Contr.*, **141**(12).
- [27] Zamani, A., and Bhounsule, P. A., 2017. "Foot placement and ankle push-off control for the orbital stabilization of bipedal robots". In Proc. IEEE/RSJ Int. Conf. Int. Robot. Syst., pp. 4883–4888.
- [28] Rijnen, M., Saccon, A., and Nijmeijer, H., 2019. "Reference spreading: Tracking performance for impact trajectories of a 1DoF setup". *IEEE Trans. Contr. Syst. Tech.*
- [29] Grizzle, J., Abba, G., and Plestan, P., 2001. "Asymptotically stable walking for biped robots: Analysis via systems with impulse effects". *IEEE Trans. Autom. Contr.*, **46**(1), pp. 51–64.
- [30] Khalil, H. K., 1996. Nonlinear control. Prentice Hall.
- [31] Galeani, S., Menini, L., and Potini, A., 2011. "Robust trajectory tracking for a class of hybrid systems: An internal model principle approach". *IEEE Trans. Autom. Contr.*, **57**(2), pp. 344–359.
- [32] Gu, Y., Yao, B., and Lee, C. S. G., 2016. "Bipedal gait recharacterization and walking encoding generalization for stable dynamic walking". In Proc. IEEE Int. Conf. Robot. Autom., pp. 1788–1793.
- [33] Gu, Y., Yao, B., and Lee, C. S. G., 2018. "Exponential stabilization of fully actuated planar bipedal robotic walking with global position tracking capabilities". *ASME J. Dyn. Syst. Meas. Contr.*, **140**(5), p. 051008.
- [34] Gu, Y., Yao, B., and Lee, C. S. G., 2017. "Time-dependent orbital stabilization of underactuated bipedal walking". In Proc. American Contr. Conf., pp. 4858–4863.
- [35] Gu, Y., Yao, B., and Lee, C. S. G., 2018. "Straight-line contouring control of fully actuated 3-d bipedal robotic walking". In Proc. Amer. Contr. Conf., pp. 2108–2113.
- [36] Iqbal, A., Gao, Y., and Gu, Y., 2020. "Provably stabilizing controllers for quadrupedal robot locomotion on dynamic rigid platforms". *IEEE/ASME Trans. Mechatron.*, **25**(4), pp. 2035–2044.
- [37] Gu, Y., and Yuan, C., 2020. "Adaptive robust trajectory tracking control of fully actuated bipedal robotic walking". In Proc. IEEE/ASME Int. Conf. Adv. Intel. Mechatron., pp. 1310–1315.
- [38] Fu, K. S., Gonzalez, R., and Lee, C. S. G., 1987. *Robotics: Control, Sensing, Vision, and Intelligence*. Tata McGraw-Hill Education.

- [39] Murray, R. M., 2017. A mathematical introduction to robotic manipulation. CRC press.
- [40] Grizzle, J. W., Chevallereau, C., Sinnet, R. W., and Ames, A. D., 2014. "Models, feedback control, and open problems of 3d bipedal robotic walking". *Automatica*, **50**(8), pp. 1955–1988.
- [41] Slotine, J.-J. E., and Li, W., 1987. "On the adaptive control of robot manipulators". *Int. J. Robot. Res.*, **6**(3), pp. 49–59.
- [42] Yao, B., 1996. "Adaptive robust control of nonlinear systems with application to control of mechanical systems". PhD thesis, University of California, Berkeley.
- [43] Ioannou, P. A., and Sun, J., 2012. *Robust adaptive control*. Courier Corporation.
- [44] Branicky, M. S., 1998. "Multiple Lyapunov functions and other analysis tools for switched and hybrid systems". *IEEE Trans. Autom. Contr.*, **43**(4), pp. 475–482.
- [45] Bainov, D., and Simeonov, P., 1993. Impulsive differential equations: periodic solutions and applications, Vol. 66. CRC Press.
- [46] Westervelt, E. R., Grizzle, J. W., Chevallereau, C., Choi, J. H., and Morris, B., 2007. Feedback control of dynamic bipedal robot locomotion, Vol. 28. CRC press.
- [47] Shih, C.-L., Grizzle, J. W., and Chevallereau, C., 2012. "From stable walking to steering of a 3D bipedal robot with passive point feet". *Robotica*, **30**(7), pp. 1119–1130.
- [48] Gao, Y., Da, X., and Gu, Y., 2020. "Impact-aware online motion planning for fully-actuated bipedal robot walking". In Proc. Amer. Contr. Conf., pp. 2100–2105.
- [49] Hamed, K. A., Kim, J., and Pandala, A., 2020. "Quadrupedal locomotion via event-based predictive control and QP-based virtual constraints". *IEEE Robot. Autom. L.*, **5**(3), pp. 4463–4470.
- [50] Ames, A. D., Xu, X., Grizzle, J. W., and Tabuada, P., 2016. "Control barrier function based quadratic programs for safety critical systems". *IEEE Trans. Autom. Contr.*, **62**(8), pp. 3861–3876.
- [51] Ames, A. D., 2014. "Human-inspired control of bipedal walking robots". *IEEE Trans. Autom. Contr.*, **59**(5), pp. 1115–1130.
- [52] Gao, Y., and Gu, Y., 2019. "Global-position tracking control of multi-domain planar bipedal robotic walking". In Proc. ASME Dyn. Syst. Contr. Conf., Vol. 59148, p. V001T03A009.